water

MDPI

Article

Analysis of Barrier Lake Breach Flood Mitigation Under Cascade Reservoirs Operation: A Case Study of the Mogangling Event, Dadu River

Zaini Chen [1], Qiaoting Qin [2,*], Jing Fu [3], Jia Li [1], Liudan Ding [1], Yao Xu [4], Daling Cao [2,*] and Jianwei Liu [2]

[1] China Energy Dadu River Hydropower Development Co., Ltd., Chengdu 610041, China; 12036139@ceic.com (Z.C.)
[2] China Institute of Water Resources and Hydropower Research, Beijing 100038, China
[3] Engineering Design & Research Institute of Sichuan University Co., Ltd., Chengdu 610065, China
[4] Sichuan Provincial Water Resources Department, Chengdu 610072, China
* Correspondence: qinqiaoting@edu.iwhr.com (Q.Q.); caodl@iwhr.com (D.C.)

Abstract

The southeastern margin of the Qinghai–Tibet Plateau is characterized by complex geological conditions and frequent disasters such as landslide-induced river blockage and subsequent barrier lake breaching. With the construction of cascade reservoirs in the basin, the potential impacts of historical barrier lakes under the current flood control system remain unclear. Reconstructing the breaching process of barrier lakes is of great guiding significance for regional flood control and disaster mitigation, risk management, and the safe operation of cascade reservoirs in the basin. In this study, the Mogangling landslide barrier lake in the Dadu River basin was selected as the research object. We constructed breach flood hydrographs for the 300 m and 600 m breach scenarios and established a one-dimensional and two-dimensional coupled hydrodynamic model of the barrier lake breach flood based on the integrated flood modeling system (IFMS). The model was used to simulate the propagation and inundation processes of the breach flood under natural propagation without reservoirs and under the joint operation of the cascade reservoirs. Spatially distributed socioeconomic data were then combined with the model to assess flood impacts and the potential disaster mitigation effect of the joint operation of the cascade reservoirs. The results show that the joint operation of the cascade reservoirs can reduce the peak discharge of the barrier lake breach flood by 30.7–97.9%, decrease the total inundated area of downstream riverside towns by 70%, and reduce the GDP losses and the affected population by 89% and 87%, respectively. In addition, artificial excavation of a spillway channel can reduce the peak discharge of the natural barrier lake breach by approximately 30%.

Keywords: barrier lake breach; Dadu River; IFMS; hazard analysis; joint operation of cascade reservoirs

Academic Editor: Cesar Andrade

Received: 23 September 2026
Revised: 29 October 2026
Accepted: 31 October 2026
Published: 3 November 2026

Copyright: © 2026 by the authors. Licensee MDPI, Basel, Switzerland. This article is an open access article distributed under the terms and conditions of the Creative Commons Attribution (CC BY) license.

1. Introduction

Barrier lakes are common geological hazards in mountainous areas, usually formed when landslides triggered by rainfall, earthquakes, snowmelt, or other factors block river channels [1,2]. Barrier lake breaching is generally characterized by strong abruptness and enormous destructive power; it can release a large volume of stored water within a short

period, generating floods with large discharges, high peak flows, and long propagation distances, thereby posing serious threats to downstream infrastructure as well as to human life and property [3–5]. The southeastern margin of the Qinghai–Tibet Plateau is densely covered by high mountains and deep valleys with large topographic relief, strong seismic activity, and complex geological environments [6,7], making it highly prone to landslides and barrier lake disasters. Large rivers such as the Jinsha River, Yalong River, Dadu River, and Min River deeply incise this region, and landslide-induced river blockage and barrier lake formation occur readily under the effects of earthquakes and intense rainfall [8,9]. Historically, this region has experienced numerous large-scale landslide-induced river blockages and barrier lake breach disasters. For example, the 1786 Mogangling landslide barrier lake event on the Dadu River caused severe casualties and property losses [10]. In 1933, the Diexi earthquake triggered multiple landslides that blocked the upper reaches of the Min River and formed several barrier lakes, some of which subsequently breached and caused severe disasters in downstream areas [11]. The 2008 Wenchuan earthquake formed 257 barrier lakes, among which the Tangjiashan barrier lake posed a major threat to downstream areas [12,13]. In 2018, two successive large-scale landslides blocked the Jinsha River at Baige, and the resulting barrier lakes and breach floods inundated multiple downstream towns, destroyed numerous bridges, houses, and farmlands, and caused substantial economic losses [14,15].

In recent decades, advances in computer technology and numerical methods have made hydrodynamic models core tools for studying flood propagation and inundation. Representative models, including the Integrated Flood Modeling System (IFMS) [16], MIKE FLOOD [17], HEC-RAS [18], and LISFLOOD-FP [19], have been developed, forming a relatively complete methodological framework. Their clear physical basis, ability to describe the spatiotemporal evolution of floods, and flexibility in scenario simulation have been central to this development. For example, IFMS, developed by the China Institute of Water Resources and Hydropower Research, includes multiple functional modules for one-dimensional river hydrodynamic simulation, two-dimensional surface flow simulation, and one- and two-dimensional coupling [20]. Currently, many scholars have used hydrodynamic models to conduct extensive research on barrier lake breach floods. Chen et al. [21] reconstructed the dam-break model of the Sedongpu landslide barrier lake on the Yarlung Tsangpo River in 2018, simulated the routing of the breach flood along the downstream channel, and analyzed the flood risk under different breach scenarios. Mei et al. [22] developed a three-dimensional numerical model based on physical principles for calculating the breach behavior and morphological evolution of landslide dams, and validation against experimental cases showed that the calculated results agree well with the experimental data. Zhang et al. [23] investigated landslide dam breaching and downstream flood propagation through a combination of physical model experiments and numerical simulations, and further analyzed the effects of channel topography and upstream inflow conditions on the breach process and flood propagation. Ma et al. [24] investigated the breach process of the Tangjiashan landslide barrier lake and its downstream impacts by coupling a dam-break model with a two-dimensional unsteady flow model. Existing studies have primarily focused on the evolution of barrier lake breaches under natural, unregulated river channel conditions, clarifying the disaster-forming mechanisms, breach modes, flood routing characteristics, and hazard assessment of barrier lakes, thereby providing an important theoretical basis and technical methods for barrier lake hazard assessment and emergency response.

However, since the 1980s, a large number of reservoirs and hydropower projects have been constructed and put into operation [25]. In particular, in the large rivers of the mountainous southwestern China, the formation of cascade reservoir systems has significantly changed the propagation characteristics of floods in natural channels. Previous

studies on barrier lake breach floods under natural channel conditions are difficult to apply to the complex hydrological evolution scenarios after the construction and operation of cascade reservoirs. Therefore, it is essential to conduct research on barrier lake breach floods under the influence of the current basin reservoirs. In recent years, some studies have begun to focus on the regulation effect of downstream reservoirs on barrier lake breach floods. Chen et al. [26] analyzed the mitigation effect of pre-releasing reservoir storage and joint operation of the cascade reservoirs in the middle Jinsha River on the Baige barrier lake breach flood. Gan et al. [27] used a one-dimensional hydrodynamic model to simulate the impacts of the Baige barrier lake breach flood under two scenarios: natural discharge and interception by a downstream high dam, and the results showed that reservoir regulation can effectively reduce the flood peak and delay the arrival time of the flood peak. Zhang et al. [28] used the DB-IWHR and HEC-RAS models to assess the risk of different emergency scenarios, including excavation of a spillway channel, removal of a downstream cofferdam, and pre-release of storage from a downstream hydropower station; the results further showed that reasonable regulation of downstream reservoirs can significantly reduce the socioeconomic impact of barrier lake breach floods. Overall, downstream reservoir projects play a crucial role in reducing breach floods and mitigating the potential impacts on downstream areas.

Although existing studies have recognized the important role of downstream reservoirs in reducing barrier lake breach flood hazard, they mainly focus on typical events in recent years with relatively complete monitoring data, and the reconstruction and analysis of major historical barrier lake breach events remain relatively limited. In particular, there is a lack of analyses that place historical extreme breach floods within the current cascade reservoir system, thereby revealing the regulation capacity of the modern basin water conservancy project system when facing historical extreme floods. Moreover, barrier lake breach floods are not only significantly affected by the regulation of cascade reservoirs, hydropower stations, and other water conservancy projects along the river [27], but are also controlled by the breach mode of the barrier dam and the channel topography [23,29]. With the continuous construction of cascade reservoir systems and the long-term evolution of channel topography and underlying surface conditions, the channel topography and engineering conditions at the time of historical barrier lake events have differed markedly from the current conditions [30], and there is insufficient understanding of the potential impacts of historical disasters under the current basin flood control system. Therefore, it is necessary to explore how the modern water conservancy project system responds to historical extreme barrier lake breach floods, and to further develop a technical pathway and methodological framework that can provide a reference for the hazard assessment, emergency regulation, and disaster prevention and mitigation of similar sudden river-blocking events.

The Dadu River basin, located on the southeastern margin of the Qinghai–Tibet Plateau, has experienced multiple barrier lake breaches in its history. With the construction of cascade reservoirs in the basin, the channel storage and release conditions and the conditions for flood propagation have changed markedly. Existing studies have not yet clarified the propagation of breach flood peaks, riverside inundation, or population and economic exposure under joint operation of the cascade reservoirs. Therefore, it is urgently necessary to assess the disaster mitigation effect of historical barrier lake breaches under the current cascade reservoir conditions in the Dadu River basin. The 1786 Mogangling barrier lake breach is one of the major documented landslide-induced river-blockage disasters in the Dadu River basin. Its breach flood propagated over a long distance along the river and severely affected downstream riverside towns and settlements. Cascade reservoirs have now been constructed upstream and downstream of the Mogangling dam site, providing conditions for analyzing the combined effects of upstream inflow reduction and

downstream flood retention. The Mogangling event therefore provides a suitable case for basin-scale analysis of the propagation characteristics of historical extreme breach floods and of the disaster mitigation effects of joint operation under current cascade reservoir conditions. On this basis, this study simulated breach flood scenarios under the current basin topography and hydraulic engineering conditions. First, two barrier lake breach scenarios were established based on historical data, and the breach discharge hydrographs were reconstructed. Second, considering IFMS has demonstrated good applicability in previous flood simulation studies [31,32], IFMS was selected to simulate the propagation of the barrier lake breach flood in river channels and floodplains. Scenarios of natural routing without reservoirs and joint operation of the current cascade reservoirs were established. The propagation and inundation characteristics of the breach flood and its impacts on downstream flood hazard and population and economic exposure were compared and analyzed. The benefits of joint operation of the cascade reservoirs were then evaluated in terms of reducing the flood peak, retaining floodwater, and mitigating flood disasters. In addition, emergency response scenarios such as the artificial excavation of a spillway channel were established to further examine how engineering interventions can mitigate barrier lake breach hazard. This study can effectively fill the gap in basin-scale hazard assessment of large barrier lake breach floods in the Dadu River basin under the current cascade reservoir conditions. It also provides a scientific reference for hazard assessment and emergency response planning for similar barrier lake disasters.

2. Materials and Methods

2.1. Overview of the Mogangling Barrier Lake

On 1 June 1786, a strong Ms 7.75 earthquake occurred in the Kangding–Moxi region, triggering a giant landslide at Mogangling in Detuo Township, Luding County [10]. The landslide mass blocked the main channel of the Dadu River and formed a large barrier lake. After impounding water for 9 days, the barrier lake began to overflow by overtopping and breached on the following day, causing catastrophic damage to riverside towns including Shimian, Ebian, Leshan, and Yibin, and resulting in more than 100,000 fatalities. It is one of the most severe documented landslide-induced river-blockage events in Chinese history. The Mogangling barrier dam is located in the lower reaches of the Dadu River at 102°09′41.19″ E and 29°37′30.73″ N. The original channel at the site is a deep U-shaped valley with a relative relief of up to 800 m. The earthquake caused instability and collapse of the high mountain slope on the right bank of the Dadu River, which rapidly blocked the river and formed the barrier lake. According to Zhao et al. [33], who investigated the depositional characteristics and formation mechanism of the Mogangling landslide, the landslide volume is approximately 45 million m^3, with a length of approximately 450 m and a width of approximately 1000 m. After more than 200 years of evolution, substantial landslide deposits remain on both banks of the river (Figure 1).

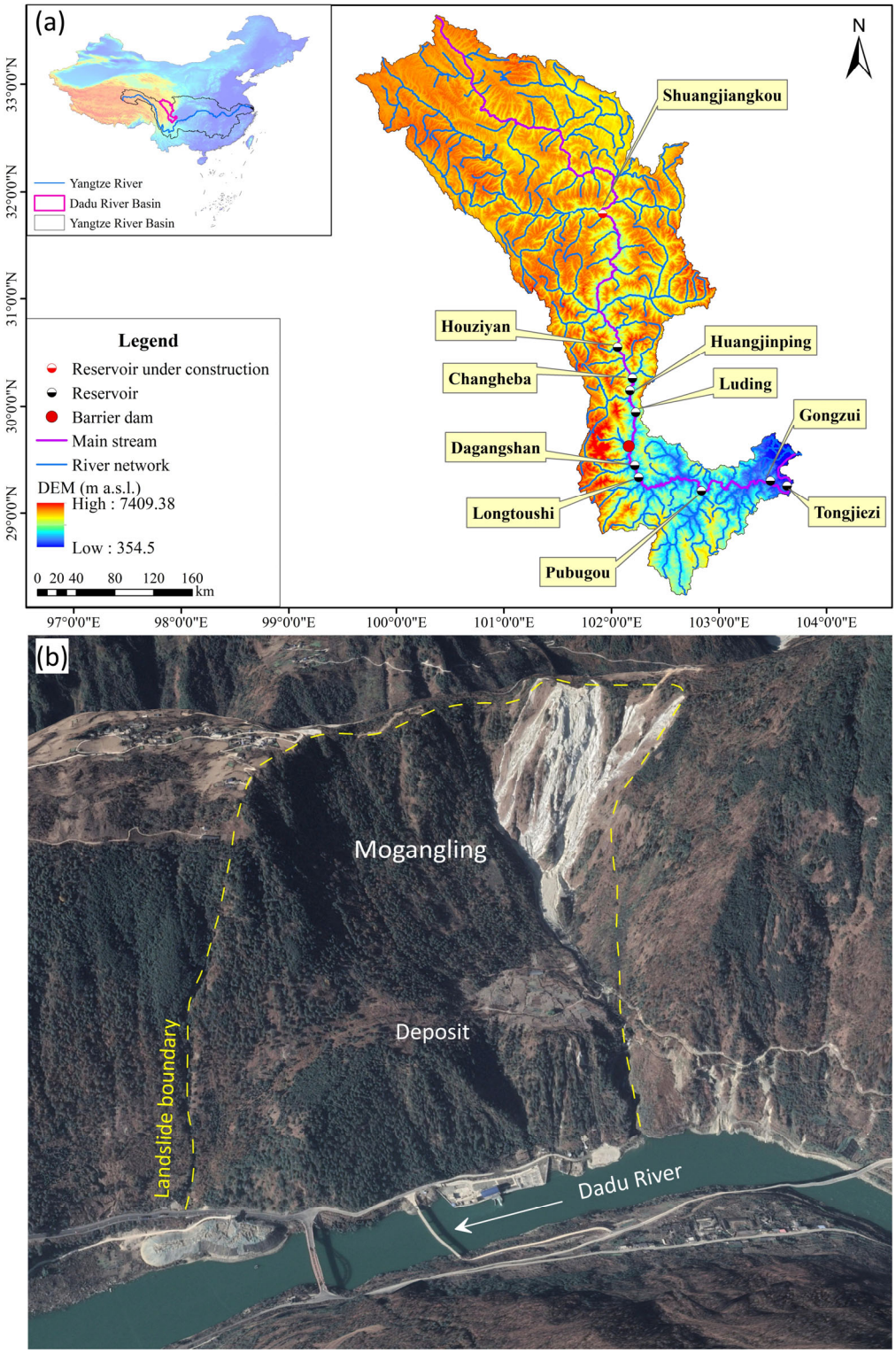


Figure 1. (**a**) Overview of the Dadu River basin and distribution of cascade reservoirs; (**b**) present-day conditions at Mogangling. The satellite image is from Google Earth.

The hydrological station nearest to the study area is the Luding station, located approximately 40 km upstream of the Mogangling barrier lake; therefore, discharges from this station were used as the inflow boundary condition. According to observed June discharges at the Luding station from 2020 to 2025, provided by the Sichuan Provincial Water

Resources Department, the annual mean June discharges ranged from 645.34 to 2889.51 m^3/s, with medians ranging from 544 to 2910 m^3/s. For June records from 2020 to 2025, the mean discharge based on valid records was 1779.46 m^3/s, and the median was 1808.8 m^3/s. Considering that the Mogangling barrier lake formed in June, a discharge of 1800 m^3/s was adopted as the representative inflow under the baseline scenario for simulations of the barrier lake breach flood and reservoir operation. Several large reservoirs, including Dagangshan, Longtoushi, Pubugou, Gongzui, and Tongjiezi, have been built in the river reach downstream of the Mogangling barrier lake, and four reservoir hydropower stations, namely Houziyan, Changheba, Huangjinping, and Luding, have been built upstream. The storage parameters of the reservoirs downstream of Mogangling are shown in Table 1 (data provided by the Sichuan Provincial Water Resources Department).

Table 1. Storage parameters of the reservoirs downstream of Mogangling.

Reservoir	Total Storage Capacity (m^3)	Regulation Storage Capacity (m^3)
Dagangshan	7.77×10^8	1.17×10^8
Longtoushi	1.40×10^8	0.17×10^8
Pubugou	50.32×10^8	10.80×10^8
Gongzui	3.10×10^8	0.96×10^8
Tongjiezi	2.02×10^8	0.55×10^8

2.2. Data

This study used DEM, land use, population grid, GDP, and building data. The 5 m DEM was obtained from the Sichuan Provincial Bureau of Surveying, Mapping and Geoinformation and represents 2020 conditions. The land use, population grid, and GDP grid data also represent 2020 conditions and were obtained from the Resource and Environment Data Cloud Platform (https://www.resdc.cn/). Land use data have a spatial resolution of 30 m, whereas the population and GDP grid data have a resolution of 1 km. Building data were obtained from the National Tibetan Plateau Data Center (https://data.tpdc.ac.cn) and represent 2023 conditions. Dataset resolutions, times, and sources are summarized in Table 2.

Table 2. Details of the datasets.

Dataset	Resolution	Time	Source
DEM	5 m	2020	Sichuan Provincial Bureau of Surveying, Mapping and Geoinformation
Land use	30 m	2020	Resource and Environment Data Cloud Platform (https://www.resdc.cn/) (accessed on 10 March 2026)
Population grid	1 km	2020	
GDP	1 km	2020	
Building	-	2023	National Tibetan Plateau Data Center (https://data.tpdc.ac.cn) (accessed on 14 March 2026)

2.3. Simulation and Hazard Analysis of the Barrier Lake Breach Flood

2.3.1. Calculation Method of the Breach Discharge Hydrograph

In this study, the DAMBRK dam-break model was used to simulate the breach discharge hydrograph. First, parameters such as the breach duration, breach side slope, breach bottom elevation, and final breach bottom width were predefined. It was assumed that breaching begins when the water level of the barrier lake exceeds a preset value, that

the breach bottom width expands from the initial state to the final bottom width within the prescribed breach duration, and that the breach bottom elevation is incised from the initial elevation to the final bottom elevation [22,34]. The breach discharge hydrograph was then calculated using the broad-crested weir formula [29]:

$$Q=3B_c(H-H_c)^{1.5}+2\tan\alpha\,(H-H_c)^{2.5} \quad (1)$$

where Q is the breach discharge; B_c is the bottom width of the broad-crested weir; H is the reservoir water level; H_c is the bottom elevation of the broad-crested weir; α is the angle between the breach side slope and the vertical direction.

The inflow and the total outflow jointly regulate the change in the storage volume of the barrier lake, satisfying the water balance equation:

$$I-Q=ds/dt \quad (2)$$

where I is the inflow discharge; Q is the total outflow; ds/dt is the rate of change of the barrier lake storage volume.

2.3.2. Development of the Hydrodynamic Model

(1) Model principles

IFMS can simulate flood propagation in river channels and the spreading of overbank flow across floodplains while calculating hydrodynamic variables such as discharge, water level, water depth, and flow velocity. Roads and levees can be represented as flow-blocking structures, and breaches, gates, and weirs can be represented as hydraulic structures. The built-in GPU acceleration strategy substantially improves computational efficiency, making IFMS a powerful tool for flood simulation. The one-dimensional hydrodynamic module describes river flow using the Saint-Venant equations, represents channel geometry and flow resistance through channel cross-sections and hydraulic parameters, and solves these equations using the Godunov scheme of the finite volume method [35]. The one-dimensional Saint-Venant equations are [36]:

$$B\frac{\partial Z}{\partial t}+\frac{\partial Q}{\partial x}=q \quad (3)$$

$$\frac{\partial Q}{\partial t}+\frac{\partial}{\partial x}\left(\frac{\alpha Q^2}{A}\right)+gA\frac{\partial Z}{\partial x}+gA\frac{|Q|Q}{K^2}=qV_x \quad (4)$$

where Q and q are discharge and lateral inflow, respectively; Z is water level; A is the channel cross-sectional flow area; α is the correction coefficient; K is the conveyance; V_x is the component of the lateral inflow velocity in the flow direction; and B is the channel water-surface width at the current water level. B is determined jointly by the cross-sectional geometry and water level and can be expressed as $B = \partial A/\partial Z$. Therefore, for natural rivers, B generally varies with longitudinal position and water level, i.e., $B = B(x,Z)$. Measured channel cross-sections were used to describe channel geometry and its longitudinal variation.

The two-dimensional hydrodynamic module is based on depth-averaged two-dimensional shallow water equations and describes flood propagation in the horizontal plane. The equations are solved numerically using the Godunov method and Roe solver, and terrain and friction source terms represent the interactions between flow and surface conditions [37]. The two-dimensional shallow water equations are [36]:

$$\frac{\partial \mathrm{h}}{\partial t}+\frac{\partial \mathrm{h}u}{\partial x}+\frac{\partial \mathrm{h}v}{\partial y}=0 \quad (5)$$

$$\frac{\partial \mathrm{h}u}{\partial t}+\frac{\partial}{\partial x}\left(\mathrm{h}u^2+\frac{1}{2}g\mathrm{h}^2\right)+\frac{\partial \mathrm{h}uv}{\partial y}=s_x \tag{6}$$

$$\frac{\partial \mathrm{h}v}{\partial t}+\frac{\partial \mathrm{h}vu}{\partial x}+\frac{\partial}{\partial y}\left(\mathrm{h}v^2+\frac{1}{2}g\mathrm{h}^2\right)=s_y \tag{7}$$

$$S_x=g\mathrm{h}\left(S_{0x}\text{-}S_{fx}\right) \tag{8}$$

$$S_y=g\mathrm{h}\left(S_{0y}\text{-}S_{fy}\right) \tag{9}$$

where h is the water depth; u is the flow velocity in the x direction; v is the flow velocity in the y direction; s_x, s_y are momentum source terms in the x and y directions, respectively; S_{0x} and S_{0y} are bed slopes in the corresponding directions; and S_{fx} and S_{fy} are friction slopes in the corresponding directions, which can be calculated using the Manning formula. The bed-slope and friction terms represent the effects of topographic gravity and bed resistance on flow, respectively.

(2) Model development

One-dimensional hydrodynamic models are suitable for simulating flood propagation in the longitudinal direction of a river and offer high computational efficiency. Two-dimensional models can characterize the spatial spreading and inundation of floodwater in floodplains but require greater computational effort. Considering the long propagation distance, complex channel topography, and possible overbank flow in local reaches of the Mogangling breach flood, this study used a coupled one- and two-dimensional hydrodynamic model. This approach balances computational efficiency for long-distance flood routing with detailed simulation of local floodplain inundation. The one-dimensional model simulated longitudinal flood propagation along the main channel of the Dadu River, while the two-dimensional model simulated the spatial spreading and inundation of overbank flow in riverside floodplains. The models were coupled by lateral connections to enable water exchange between the channel and floodplain.

Considering the attenuation characteristics of the flood along the river, the Mogangling barrier lake dam site was taken as the starting point of the model and Jiang'an County in Yibin City as the end point of the model. The modeling area includes key riverside towns such as Detuo, Shimian, Hanyuan, Jinkouhe, Shawan, Leshan, Wutongqiao, Qianwei, and Yibin (Figure 2). The one-dimensional hydrodynamic model covers a channel length of 586.6 km with 1998 cross-sections, and the average cross-section spacing is about 300 m. For the two-dimensional surface model, combined with the actual terrain and the distribution of riverside towns, a range of 3–6 km on the left and right banks of the main Dadu River was selected, with a modeling area of about 3550 km^2. The modeling area was meshed with a grid size of 100 m, and the grids within 2 km of the important towns and the two river banks were refined to a grid size of 20 m, resulting in a total of 1.26 million grids. A 5 m resolution DEM was used to interpolate the elevation of the grid cells, the roughness was assigned according to the land use type with a value range of 0.03–0.12 (Table 3), and the grid edge elements were corrected according to the levee flood control standard. Initial water levels and discharges in the one-dimensional channel were determined by steady-state calculations under prescribed background discharges and used as the initial conditions for unsteady flow simulation. The two-dimensional floodplain was initially set as dry land with zero flow velocity. The upstream boundary used the calculated barrier lake breach discharge hydrograph, and the downstream boundary used a free-outflow condition. The total simulation duration was 96 h, with a computational time step of 10 s.

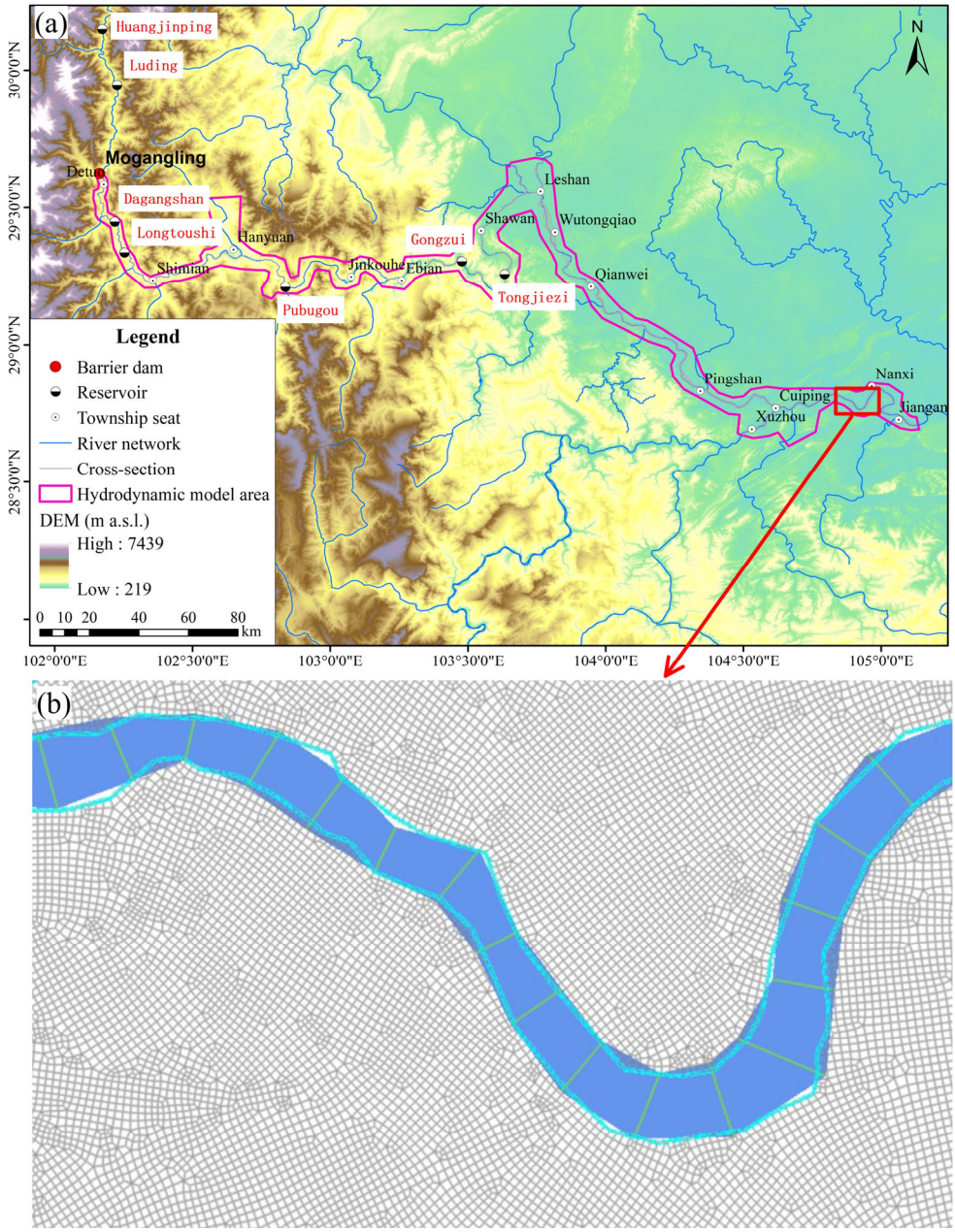


Figure 2. (**a**) Model domain; (**b**) local view of the 1D–2D coupling.

Table 3. Roughness coefficients for different land use classes.

Land Use Class	Roughness Coefficient
Paddy field	0.04
Dry farmland	0.06
Urban land	0.12
Rural residential area	0.09
Other construction land	0.12
Forest land	0.10
Grassland	0.08
Water body	0.03
Unused land	0.06

(3) Flood inundation depth classification method

This study followed the approach of Beden et al. [38] and Peker et al. [39] to classify flood hazard based on inundation depth and developed a depth-classification scheme suitable for the scenario comparisons in this study by considering the characteristics of barrier lake breach floods. Compared with basin rainstorm floods, barrier lake breach floods are typically more abrupt, have larger peak discharges, rise and fall sharply, and have shorter durations; local inundation depths can also be large in mountainous gorge terrain. Because this study focused on the inundation intensity of extreme breach floods and the response to reservoir operation measures, the maximum inundation depth was divided into six intervals: <2.0 m, 2.0–5.0 m, 5.0–10.0 m, 10.0–15.0 m, 15.0–20.0 m, and >20.0 m, which were designated Grades I–VI, respectively (Table 4).

Table 4. Classification of maximum inundation depth.

Flood Depth (m)	Level
<2.0	I
2.0–5.0	II
5.0–10.0	III
10.0–15.0	IV
15.0–20.0	V
>20.0	VI

2.3.3. Development of the Flood Impact and Loss Assessment Model

Flood impact analysis was carried out using spatial overlay and aggregation statistics methods. By spatially overlaying the flood inundation extent, administrative boundaries, and land use data, a refined spatial dataset with topological information was constructed; combined with socioeconomic data and flood inundation parameters, flood impact indicators by administrative region, land use type, and hazard-bearing body were obtained through aggregation statistics, including the inundation area, affected population, affected townships and affected villages.

Flood loss assessment adopted the loss-ratio curve method [40]. This method establishes relationships between flood inundation depth and the relative loss ratios of hazard-bearing bodies, thereby reflecting possible asset-value losses under different inundation conditions. Existing studies have generally established relationships between loss ratios and indicators such as inundation depth for different hazard-bearing bodies based on historical disaster loss surveys, insurance claim data, field surveys, expert judgment, and comprehensive analysis [41,42]. This study used loss-ratio curves provided by the Sichuan Provincial Water Resources Department, as shown in Figure 3. The flood loss ratio is defined as the ratio of the value lost by a hazard-bearing body under flood impact to its pre-disaster asset value and is calculated as follows:

$$L=\frac{S_0\text{-}S_1}{S_0} \quad (10)$$

where L is the loss ratio of a certain type of property; S_0 is the pre-disaster value of the property; S_1 is the post-disaster value of the property.

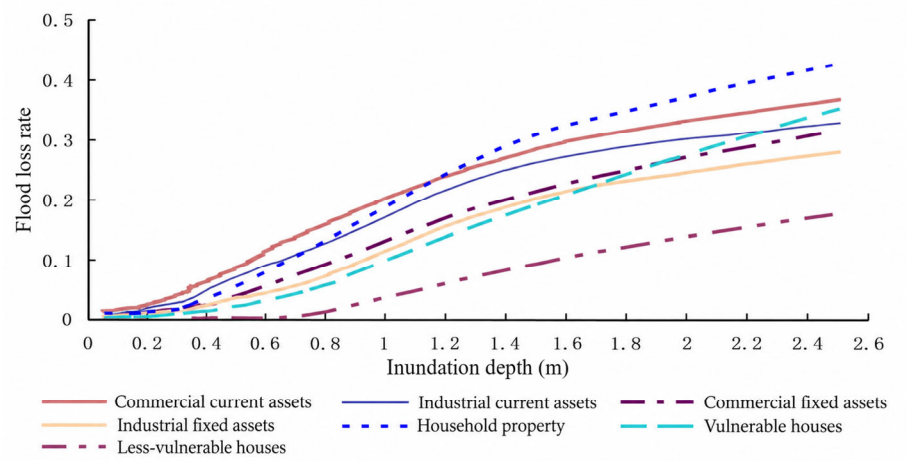


Figure 3. Flood loss-rate curves.

2.4. Joint Operation Scheme of Cascade Reservoirs Under the Breach Flood

To respond to the sudden breach flood of the Mogangling barrier lake and to reduce the flood hazard of the downstream channels, towns, and cascade hydropower stations, a multi-reservoir coordinated joint operation scheme of "pre-releasing storage upstream, peak staggering and peak reduction step by step, impoundment by core reservoirs, and auxiliary flood control by downstream reservoirs" was formulated, which maximizes the comprehensive disaster mitigation efficiency of the reservoir group through advance pre-release, graded regulation, and coordinated flood retention (Figure 4). The pre-release discharges set for the reservoirs are 2000 m^3/s for Dagangshan, 3000 m^3/s for Longtoushi, 4000 m^3/s for Pubugou, 5000 m^3/s for Gongzui, and 5500 m^3/s for Tongjiezi, by releasing water in advance to vacate reservoir storage for flood retention. Among them, the Dagangshan and Longtoushi reservoirs respond the fastest and can be quickly drawn down to the dead water level within 24 h; the operation periods of the downstream Gongzui and Tongjiezi reservoirs are relatively long, and they can be steadily drawn down to the dead water level within 48 h to complete storage release; the core regulating reservoir Pubugou can add 80 million m^3 of regulation storage per day; and the Dagangshan reservoir can be continuously operated for 96 h to reach the limit dead water level. The above reservoirs vacate a total of 620 million m^3 of storage, providing sufficient storage space for flood retention. Considering that the upstream hydropower stations are primarily used for power generation and have relatively limited regulation capacity, while also ensuring the basic ecological flow requirements of the upstream river reaches, this study establishes a reference scenario in which upstream reservoir operations reduce the inflow discharge by 20%. With this reduction from the June average inflow of 1800 m^3/s, the inflow into the barrier lake is calculated as 1440 m^3/s.

When the barrier lake breach flood propagates downstream, the reservoir group activates a graded coordinated regulation mechanism, forming a flood control system with layered defenses. First, the most upstream Dagangshan and Longtoushi reservoirs release water at their maximum discharge capacity to stagger the peak, carrying out the first round of peak reduction on the breach flood; the residual flood after the initial regulation by the Dagangshan reservoir can be completely retained by the Pubugou reservoir, realizing effective control of the breach flood; the downstream Gongzui and Tongjiezi reservoirs, as the last flood control barrier, maintain low-level operation throughout the process and reserve sufficient flood control storage, assisting in retaining the residual flood and steadily regulating the downstream channel water level to avoid flood overbanking and inundation. The overall operation process realizes the temporal coordination and

functional complementarity of the upstream and downstream reservoirs, retaining the breach flood step by step, effectively controlling the flood hazard, and greatly reducing the hazard of downstream channel inundation, town disasters, and damage to and shutdown of cascade hydropower stations.

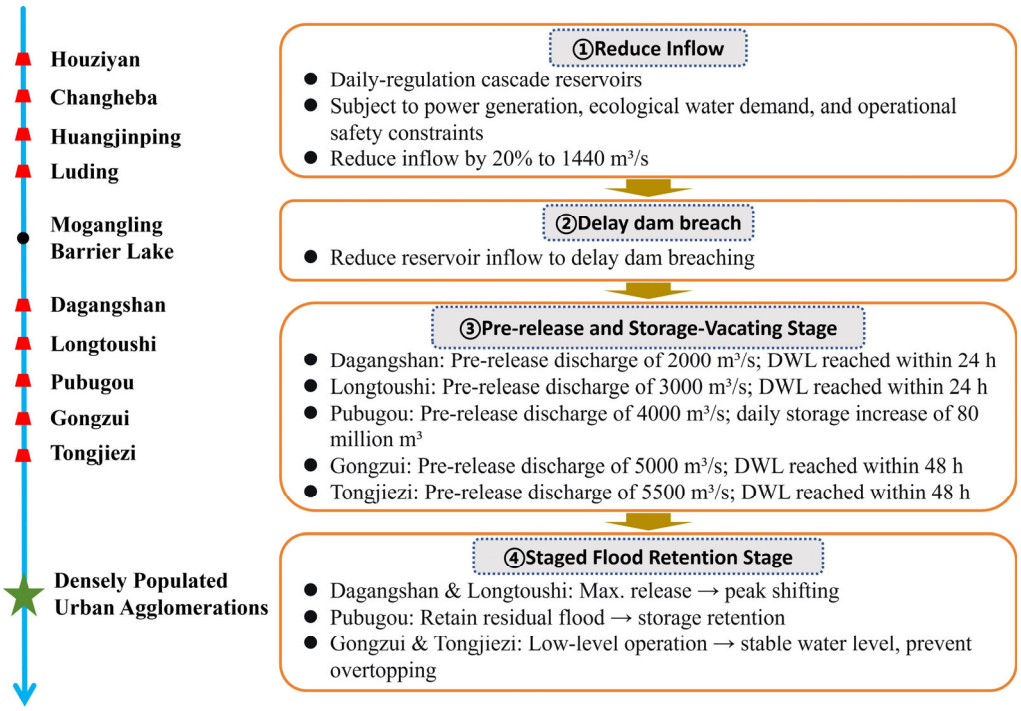


Figure 4. Flowchart of the joint operation sequence of the Dadu River cascade reservoirs.

3. Results

3.1. Simulation of the Breach Discharge Hydrograph

Through investigation and analysis of the existing literature and topographic changes [10,33,43], the breach shape and development process at the time of the barrier lake breach were inferred, and the backwater inundation extent and storage capacity curve were derived in combination with the current topographic elevation (Figure 5). The calculation results show that the backwater length upstream of the barrier dam is about 34.7 km, and the upstream end of the backwater extends to Luqiao Town in Luding County, affecting Jiajun Township, Lengqi Town, and Chuni Township.

On the basis of the existing literature on Mogangling, and combined with an analogy analysis of typical barrier lake breach events such as Tangjiashan and Baige, the breach parameters of the Mogangling barrier dam were comprehensively determined. It is estimated that the total storage capacity of the Mogangling barrier lake is about 1.15 billion m³, the dam height is about 167 m, the overtopping breach water level is about 1300 m, the breach bottom width is about 300–600 m, and the breach duration is about 5–10 h. Therefore, two breach simulation scenarios were set in this study: Scenario 1 is the most likely breach scenario, with a breach bottom width of 300 m and a breach duration of 10 h, giving a simulated peak discharge of 67,100 m³/s; Scenario 2 is the most unfavorable scenario, with a breach bottom width of 600 m and a rapid breach duration of 5 h, corresponding to an extreme flood peak discharge of up to 128,400 m³/s. This study assumes progressive breach development, with the breach geometry evolving continuously over the prescribed breach duration. The breach discharge is calculated using the barrier lake water level–storage relationship and the broad-crested weir equation. The resulting

breach hydrograph is output at variable time intervals, with a 1 min interval during the first 8 h and a 5 min interval during the subsequent 8 h. The breach processes of the two scenarios are shown in Figure 6.

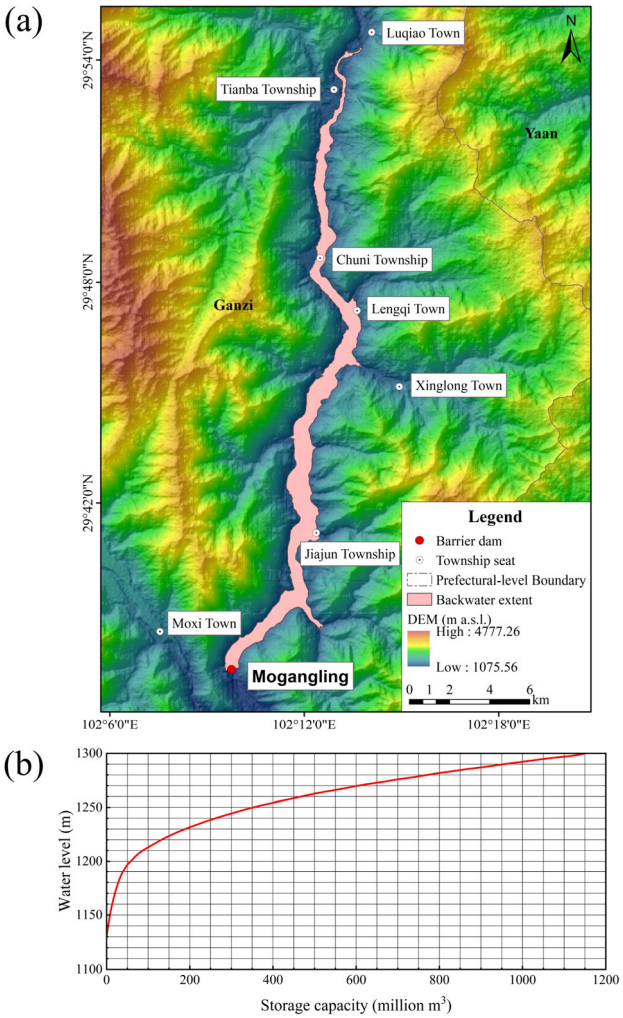


Figure 5. Mogangling barrier lake: (**a**) backwater inundation extent; (**b**) water level–storage capacity curve.

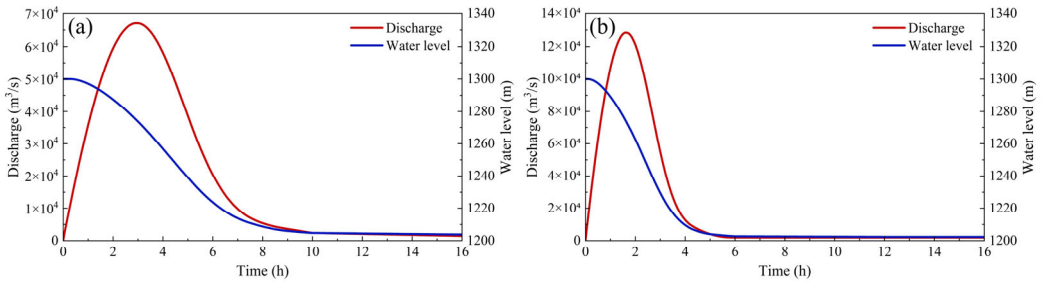


Figure 6. Breach flood hydrographs under different breach-width scenarios: (**a**) 300 m; (**b**) 600 m.

3.2. Simulation of the Breach Flood Routing

The breach discharge hydrographs obtained above for the 300 m and 600 m breach scenarios were used as boundary conditions to drive the hydrodynamic model, and the inundation under the no-reservoir natural routing and cascade reservoir impoundment

scenarios was simulated separately. Figure 7 shows the inundation extent and water depth distribution in the reach above Pubugou under the 300 m and 600 m breach scenarios, with and without cascade reservoir regulation. Under the cascade reservoir impoundment scenario, the breach flood passes through the Dagangshan and Longtoushi reservoirs and is finally completely retained at the Pubugou reservoir; under the no-reservoir impoundment condition, the breach flood continues to propagate downstream after passing through the Pubugou reservoir. Affected by factors such as channel regulation, valley widening, and flood propagation attenuation along the river, the overall inundation extents under the 300 m and 600 m breach scenarios are relatively consistent, and the difference is mainly reflected in that the inundation depth along the river under the 600 m breach scenario is generally higher than that under the 300 m breach scenario, with the difference in inundation depth between the two breach scenarios being most obvious under the no-reservoir regulation scenario.

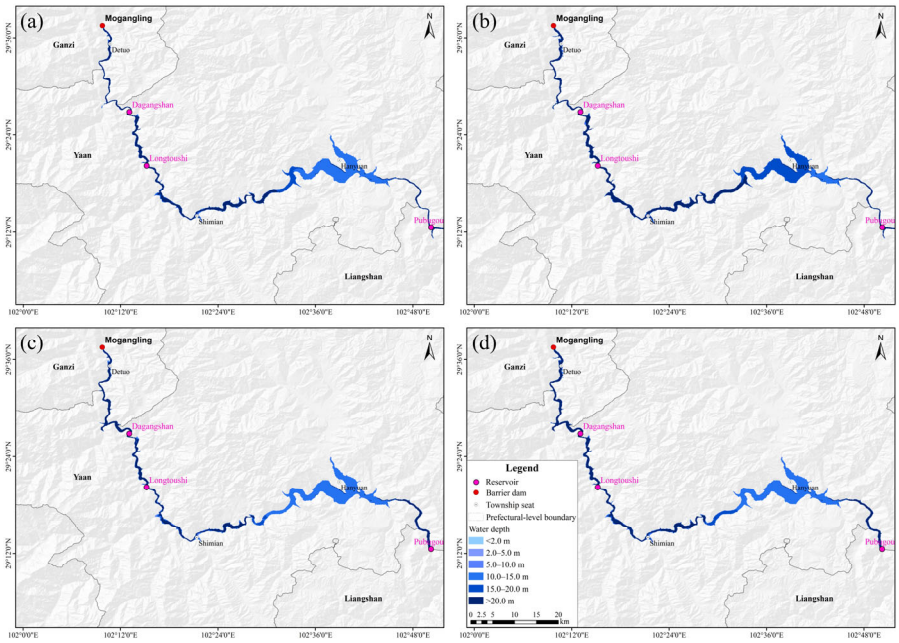


Figure 7. Distribution of maximum inundation depth in the reach above Pubugou under different breach widths and reservoir regulation scenarios: (**a**) 300 m breach width without reservoir regulation; (**b**) 600 m breach width without reservoir regulation; (**c**) 300 m breach width with reservoir regulation; (**d**) 600 m breach width with reservoir regulation.

To further analyze the influence of cascade reservoir regulation on the flood inundation characteristics of key riverside towns, taking the 600 m breach scenario as an example, the maximum inundation depths of riverside towns such as Detuo, Shimian, and Hanyuan under the with- and without-reservoir regulation conditions were compared and analyzed (Figure 8). It can be seen that the responses of different areas to reservoir regulation show obvious spatial differences. Detuo is located near the downstream of the Mogangling barrier dam and in the upstream part of the cascade reservoirs, so the inundation extent and water depth distribution under the with- and without-reservoir scenarios are generally similar. As the breach flood propagates downstream and gradually passes through the cascade reservoir regulation, the peak-reduction effect of the reservoirs gradually emerges. After being retained by the Dagangshan and Longtoushi reservoirs, the inundation depths of Shimian and Hanyuan decrease significantly, and the inundation extents are also relatively small.

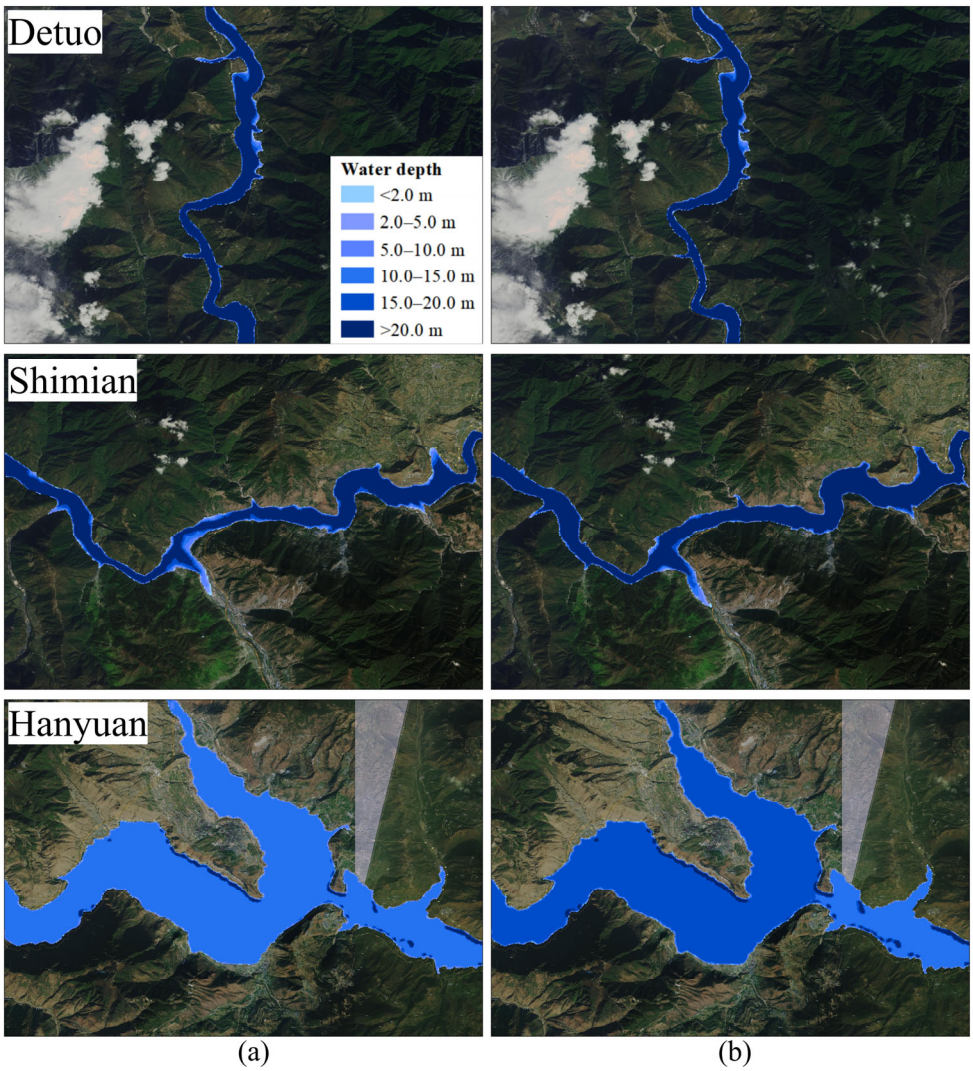


Figure 8. Inundation depth of riverside towns upstream of Pubugou under the 600 m breach-width scenario: (**a**) with reservoir impoundment; (**b**) without reservoir impoundment.

Under the no-reservoir regulation scenario, after passing through the Pubugou reach, the Mogangling barrier lake breach flood continues to propagate downstream along the Dadu River and successively affects riverside towns such as Jinkouhe, Shawan, Leshan, Wutongqiao, and Qianwei, and is finally completely attenuated by the time it reaches Yibin (Figure 9). Because of the long-distance propagation and the influence of factors such as channel regulation and valley widening along the river, the differences between the two breach scenarios gradually weaken. The overall propagation paths and inundation extents of the floods under the 300 m and 600 m breach scenarios are basically consistent, and the changes in inundation depth are also relatively small.

Taking the 600 m breach scenario as an example, inundation characteristics varied markedly among different river reaches, and flood arrival times also differed considerably (Figure 10). Jinkouhe is located in a deeply incised gorge with steep terrain on both banks, where the inundation depth within the channel was relatively large; the flood arrival time (FAT) was 14.2 h. After passing Shawan, the flood began to enter the plain area, the inundation depth decreased markedly, and the inundation extent expanded. Low-lying areas along both banks of Shawan, Leshan, and Wutongqiao were inundated, with FATs of 28.4 h, 31.7 h, and 34.5 h, respectively. Owing to flood peak attenuation and the longitudinal

spreading of floodwater during long-distance propagation, the breach flood reached Qianwei after 37.8 h, where only limited inundation occurred. The breach flood reached Yibin after 51.2 h and was completely attenuated there.

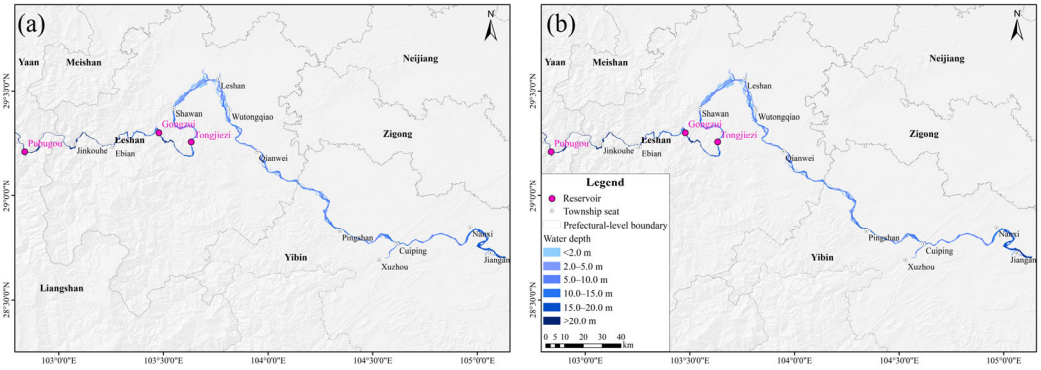


Figure 9. Distribution of maximum inundation depth in the reach below Pubugou for different breach widths: (**a**) 300 m; (**b**) 600 m.

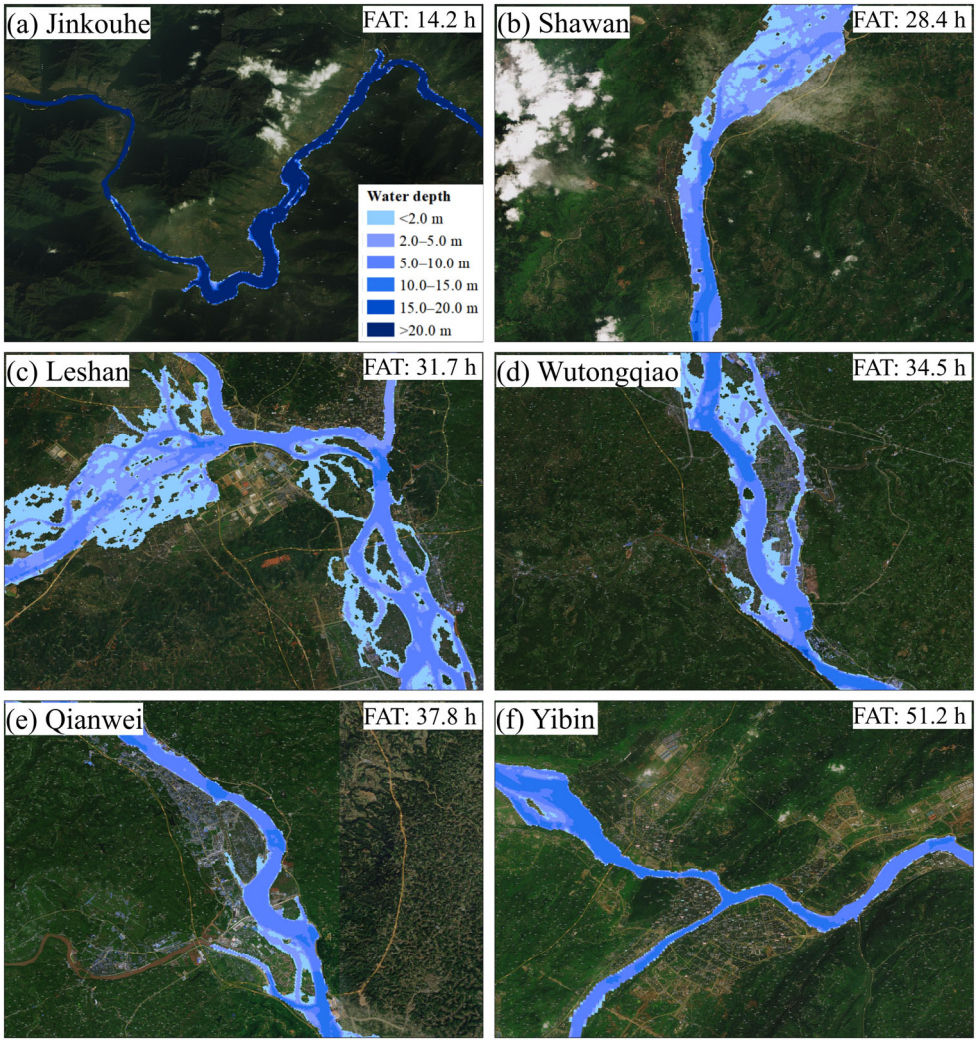


Figure 10. Inundation of riverside towns downstream of Pubugou under the natural routing scenario (600 m breach width): (**a**) Jinkouhe; (**b**) Shawan; (**c**) Leshan; (**d**) Wutongqiao; (**e**) Qianwei; (**f**) Yibin.

3.3. Flood Hazard Analysis Under Different Scenarios

The flood inundation disaster losses under the 300 m and 600 m breach scenarios, under the no-reservoir natural routing and with-reservoir impoundment scenarios, were evaluated (Table 5). Under the 300 m breach scenario, the inundation areas under the no-reservoir natural routing and with-reservoir impoundment scenarios were 361.58 km^2 and 107.75 km^2, respectively; the numbers of affected townships were 111 and 21, respectively; the numbers of affected villages were 469 and 71, respectively; the numbers of inundated buildings were 3701 and 843, respectively; the affected populations were 77,259 and 9464 persons, respectively; and the GDP losses were 388,705 × 10^4 CNY (58,091.97 × 10^4 USD, the reference exchange rate on October 16, 2026, was adopted at 1 USD = 6.6912 CNY) and 43,378 × 10^4 CNY (6482.84 × 10^4 USD), respectively. Under the 600 m breach scenario, the inundation areas under the no-reservoir natural routing and with-reservoir impoundment scenarios were 365.52 km^2 and 109.94 km^2, respectively; the numbers of affected townships were 111 and 21, respectively; the numbers of affected villages were 471 and 72, respectively; the numbers of inundated buildings were 3787 and 903, respectively; the affected populations were 77,693 and 9947 persons, respectively; and the GDP losses were 390,087 × 10^4 CNY (58,298.51 × 10^4 USD) and 44,118 × 10^4 CNY (6593.44 × 10^4 USD), respectively.

Through comparative analysis of the statistical results, compared with the natural flood routing scenario, under the joint operation of the cascade reservoirs the inundation area of the breach flood was reduced by about 70%; the GDP loss was reduced by about 89%; the affected population was reduced by about 87%; the number of affected townships was reduced by about 81%; the number of affected villages was reduced by about 85%; and the number of inundated buildings was reduced by about 76%.

Table 5. Comparative analysis of disaster losses under different scenarios.

	300 m Breach Scenario		**600 m Breach Scenario**	
	with Reservoirs	**Without reservoirs**	**with Reservoirs**	**Without Reservoirs**
Inundated area (km^2)	107.75	361.58	109.94	365.52
GDP loss (×10^4 CNY [×10^4 USD])	43,378 [6482.84]	388,705 [58,091.97]	44,118 [6593.44]	390,087 [58,298.51]
Affected population (persons)	9464	77,259	9947	77,693
Affected townships (No.)	21	111	21	111
Affected villages (No.)	71	469	72	471
Inundated buildings (No.)	843	3701	903	3787

For the most unfavorable Scenario 2, the water level and discharge routing processes at key cross-sections along the river under the with- and without-reservoir regulation conditions were compared and analyzed (Figure 11). The results show that the flood peak discharge and water level processes at the cross-sections differ significantly between the two conditions: under the no-reservoir condition, the flood peak discharges at the Detuo, Dagangshan, Longtoushi, Shimian, Hanyuan, and Pubugou cross-sections were 121,735 m^3/s, 121,029 m^3/s, 113,744 m^3/s, 94,320 m^3/s, 60,609 m^3/s, and 31,650 m^3/s, respectively. Under the joint impoundment of the cascade reservoirs, the flood peak discharges at the above cross-sections became 121,726 m^3/s, 83,922 m^3/s, 73,523 m^3/s, 60,930 m^3/s, 32,106 m^3/s, and 659 m^3/s, respectively. The comparison shows that the flood peak discharges at the Dagangshan, Longtoushi, Shimian, Hanyuan, and Pubugou cross-sections were reduced by 30.7%, 35.4%, 35.4%, 47.0%, and 97.9%, respectively.

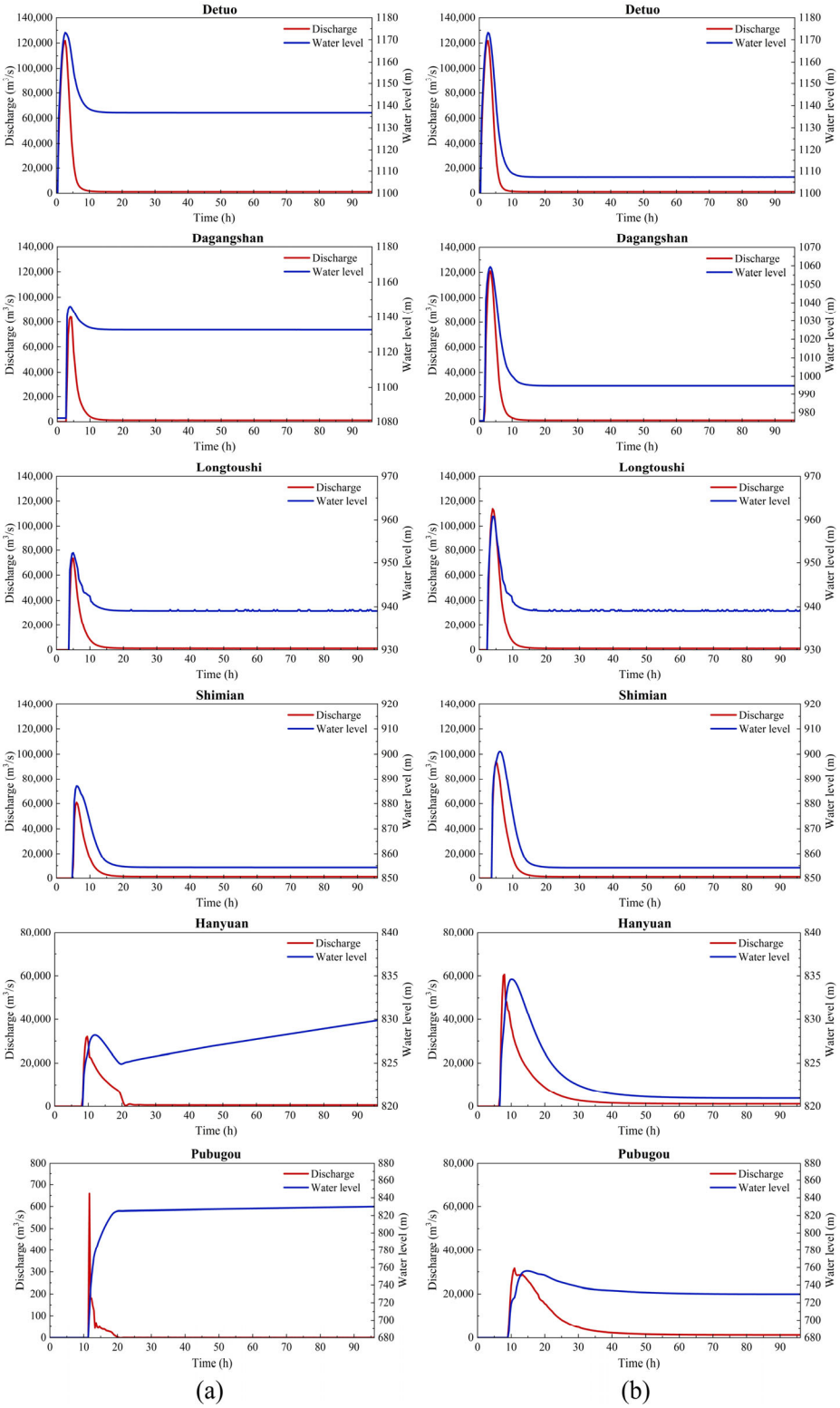


Figure 11. Water level and discharge hydrographs at key cross-sections under Scenario 2 (600 m breach width): (**a**) with reservoirs; (**b**) without reservoirs.

It can be seen that the Detuo cross-section near the barrier dam site upstream is relatively less affected by reservoir regulation; after the flood enters the reach regulated by the cascade reservoirs, the flood peak attenuates significantly along the river, and the Pubugou reservoir shows the most prominent peak-reduction effect, being able to almost

completely retain the breach flood. Overall, the basin cascade reservoirs have a strong capacity for peak reduction, flood retention, and peak staggering of the barrier lake breach flood, significantly reducing the overall flood hazard of the basin.

Under the no-reservoir impoundment condition, the Mogangling barrier lake breach flood continuously propagates downstream along the channel, causing increases in discharge and rises in water level at key cross-sections downstream of the Pubugou reservoir; the flood routing processes at these cross-sections are shown in Figure 12. The flood peak discharges at the Jinkouhe, Gongzui, Tongjiezi, Shawan, Leshan, Wutongqiao, Qianwei, and Yibin cross-sections were 14,493 m^3/s, 16,763 m^3/s, 15,106 m^3/s, 13,789 m^3/s, 14,025 m^3/s, 12,920 m^3/s, 12,373 m^3/s, and 7778 m^3/s, respectively. During the routing of the breach flood along the river, there is a certain degree of attenuation and peak-time lag, but the middle and lower reaches such as Jinkouhe, Gongzui, Tongjiezi, Shawan, Leshan, Wutongqiao, and Qianwei still maintain high flood peak discharges, and the flood has a strong disaster-causing capacity. Therefore, without the impoundment of the cascade reservoirs, the towns along the middle and lower Dadu River and the main Min River would face considerable flood conveyance pressure and flood control pressure.

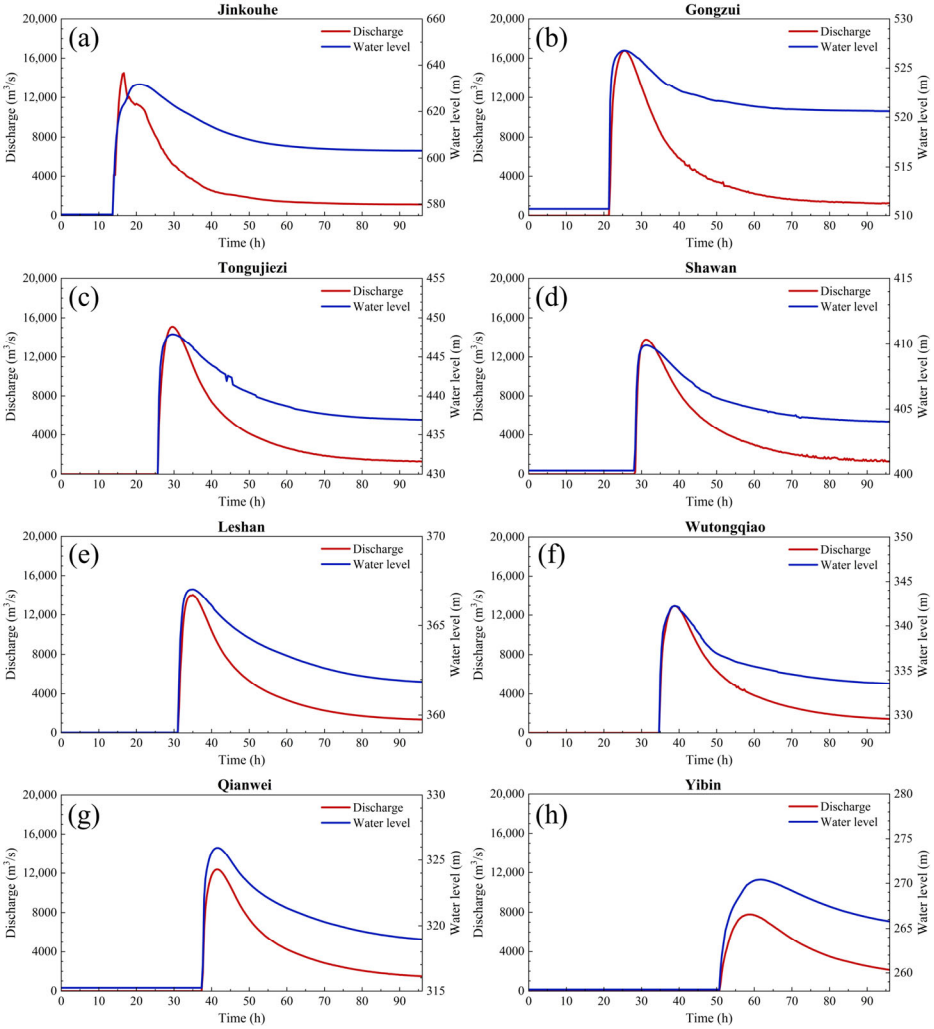


Figure 12. Water level and discharge hydrographs at key cross-sections downstream of Pubugou under Scenario 2 (600 m breach width) without reservoirs: (**a**) Jinkouhe; (**b**) Gongzui; (**c**) Tongjiezi; (**d**) Shawan; (**e**) Leshan; (**f**) Wutongqiao; (**g**) Qianwei; (**h**) Yibin.

4. Discussion

4.1. Disaster Mitigation Effect of Joint Operation of Cascade Reservoirs

Under the current water conservancy project conditions in the basin, if a large barrier lake similar to Mogangling were to form and breach again, it could still pose serious flood hazard to the riverside towns upstream and downstream. With the continuous advancement of urbanization in the basin, the population, towns, and important infrastructure along the Dadu River and its downstream reaches are highly concentrated, the exposure to flood disasters keeps rising, and the vulnerability and potential losses of the riverside towns also increase accordingly. In recent years, extreme weather events have shown a trend of frequent and repeated occurrence [44], with their abruptness, extremity, and abnormality continuously intensifying [45], which places higher demands on basin flood control safety and the emergency operation of water projects. The comprehensive basin emergency joint operation, considering upstream reservoir interception and downstream reservoir impoundment, reduced the barrier lake breach hazard by more than 70%, indicating that the joint operation of cascade reservoirs significantly enhances the capacity of the basin to respond to extreme events. Existing studies have shown that cascade reservoirs play a crucial role in the basin flood control system. Upstream reservoirs can reduce the inflow intensity by regulating the released discharge, thereby relieving the flood control pressure on downstream channels and control projects [46,47]; downstream reservoirs can reduce the impact of floods on downstream riverside towns and important infrastructure through advance pre-release of storage, flood peak retention and reduction, peak-staggering operation, and flood volume redistribution [26,48]. In the Dadu River basin, with the operation of the upstream Shuangjiangkou reservoir, the inflow discharge can be further reduced in future scenarios when a flood event of the same magnitude occurs, thereby further reducing the flood hazard.

However, the disaster mitigation effectiveness of water projects in extreme sudden-onset disasters is determined not only by the project scale and storage capacity but is also jointly constrained by multiple factors such as the spatial layout of projects, storage and release capacity, and coordinated operation of multiple projects. Chou and Wu [49] pointed out that reservoir pre-release can vacate storage in advance and increase flood regulation space. During the 2020 Yangtze River floods, the 22 upstream cascade reservoirs significantly reduced the flood peaks through advance storage release, graded impoundment, and peak-staggering operation, and effectively relieved the flood control pressure in the middle and lower reaches [50]. This case shows that sufficient water project conditions and multi-department coordination are important prerequisites for fully realizing the flood control potential of reservoir groups. In contrast, retrospective studies of historical floods also show that when the spatial configuration of water projects is insufficient, the potential mitigation benefits of reservoirs may be difficult to fully realize. In the great 2011 Thailand flood, the huge downstream flood volume mainly originated from local rainfall and was outside the control range of the two upstream reservoirs; even if the operation of the two large reservoirs had been changed, the downstream inundation area would have been reduced by only about 3.68% at most [51]. This indicates that the mitigation effect of reservoir operation has clear spatial boundaries, and especially when a large amount of disaster-causing water originates from local rainfall outside the reservoir control range, relying only on upstream reservoirs is often insufficient to achieve the desired mitigation effect. Unlike the 2011 Thailand flood, the main disaster-causing flood volume of the Mogangling barrier lake was concentrated and released in the main Dadu River, and multiple cascade reservoirs, such as Longtoushi, Dagangshan, and Pubugou, have already been built downstream, so the project system has a high degree of spatial

overlap with the main flood propagation path. Therefore, the purpose of the scenario reenactment of this historical extreme event under modern conditions is not to precisely reproduce the disaster process of 1786, but to use a real extreme event to test the emergency regulation capacity of the current basin flood control system when facing unconventional sudden floods.

On the basis of fully utilizing the regulation potential of the existing cascade reservoirs in the basin, for sudden extreme disasters such as barrier lakes, emergency engineering measures such as excavation of a spillway channel on the barrier dam and temporary diversion can also be comprehensively adopted according to the disaster evolution stage, so as to further reduce the intensity of the disaster source, cut the breach flood peak, and alleviate the downstream flood hazard. The emergency response practices for barrier lakes such as Tangjiashan and Baige show that the artificial excavation of a spillway channel can lower the barrier lake water level and the water volume to be released in advance, and reduce the breach flood peak by controlling the overtopping location and the breach evolution process [52,53]. For the Baige "11·03" barrier lake, excavation of a spillway channel about 13.5 m deep reduced the breach flood peak by about 24% [53], demonstrating the important role of proactive engineering disposal in reducing barrier lake breach hazard. In this study, referring to the emergency excavation approach of the Baige barrier lake and comprehensively considering the traffic conditions, construction organization, and emergency rescue capacity in the Mogangling area, 30 excavators were set to work continuously for 3 days to excavate a spillway channel 100 m wide and 10 m deep on the barrier dam (Figure 13). The results show that under this scenario, after the barrier lake water level rose to about 1270 m, overtopping and discharge occurred about 2.5 days later, and the breach discharge hydrograph after excavation of the spillway channel is shown in Figure 13b. The breach flood peak discharge was about 47,000 m^3/s, about 30% lower than the 67,100 m^3/s of the most likely breach scenario, indicating that excavation of the spillway channel can release part of the water volume in advance and constrain the breach development process, effectively reducing the breach flood peak and regulating the breach flood hydrograph. Under the combined conditions of spillway channel excavation and advance pre-release of the reservoir group, the Mogangling barrier lake breach flood can be more fully regulated and its peak more fully reduced and absorbed along the river. Compared with the natural breach scenario, under the combined regulation condition the Longtoushi reservoir can avoid breaching, and the downstream flood peak, water level, inundation extent, and disaster losses can all be further reduced. Therefore, in the disposal of extreme sudden events, combining the joint operation of the basin cascade reservoirs with emergency engineering measures can further tap the flood control potential of the basin.

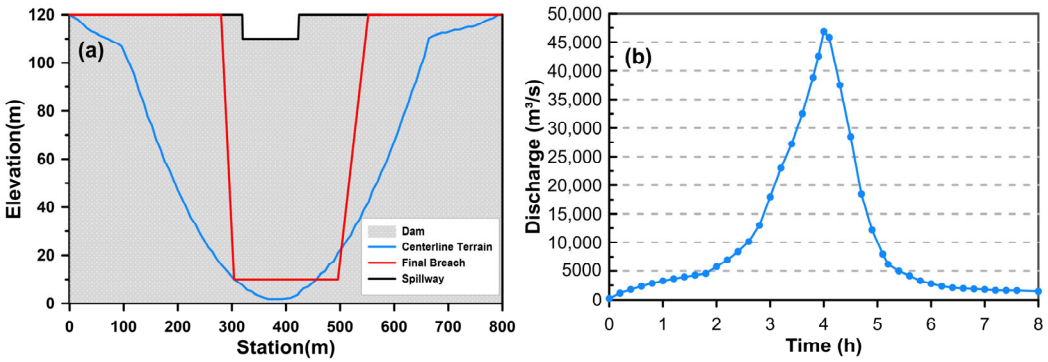


Figure 13. (**a**) Breach geometry of the Mogangling barrier dam; (**b**) breach discharge hydrograph after artificial intervention.

4.2. Uncertainty and Limitation

This study reconstructed breach flood scenarios for the 1786 Mogangling barrier lake under current topographic and reservoir conditions using the coupled IFMS one- and two-dimensional hydrodynamic model to analyze the potential disaster mitigation benefits of joint operation of the cascade reservoirs. Because the historical event occurred long ago and observational conditions were limited, continuous measurements of water level, discharge, breach evolution, and inundation are unavailable. Reconstruction of the disaster process therefore relies mainly on historical documents, disaster records, and residual geomorphic evidence [10,54]. Accordingly, uncertainty in this study mainly arises from breach-process reconstruction, terrain representation and hydrodynamic parameterization, reservoir operation conditions, and estimates of exposure and economic loss.

First, uncertainty exists in the reconstruction of the breach flood process. Parameters such as the barrier dam geometry, initial reservoir water level, breach width, breach depth, and breach duration are important for determining the breach flood process. In the absence of historical measurements, these parameters usually need to be estimated from literature, empirical relationships, topographic inversion, or physical models [55,56]. In this study, some parameters were determined from historical records, existing research, and relevant topographic conditions; however, these estimates cannot fully capture the internal structure, material composition, and breach development of the historical barrier dam. Uncertainty in these parameters may affect the breach peak discharge, total outflow, and shape of the flood hydrograph and may propagate through the inflow boundary to the downstream flood routing and inundation simulations. In addition, this study presents a scenario reenactment that places a historical disaster event under current basin conditions. Although the study area is located in a high-mountain gorge with a relatively stable river, more than two centuries have elapsed since the event; the basin DEM, local landforms, channel morphology, vegetation cover, underlying surface conditions, and hydrological and climatic characteristics may therefore have changed to varying degrees [57,58]. Therefore, even if landslide-induced river blocking were to occur again at the same location in the future, the landslide volume, barrier dam morphology, and breach mode may not be exactly the same as those of the historical event.

Second, terrain representation and hydrodynamic parameter settings may introduce uncertainty. The model was constructed using existing high-resolution topographic data and measured channel cross-sections, and local grid refinement was used to improve terrain representation in key areas. However, owing to limitations in the accuracy of the underlying data, computational scale, and the schematization of engineering structures, the local flow-blocking effects of some bridges, buildings, and other small-scale structures were not fully represented, which may affect simulated local water levels, flow velocities, and inundation extents [59]. Manning roughness coefficients were assigned empirically based mainly on land use type, land cover characteristics, and existing literature. Because measured data were insufficient for fully calibrating the model under the scenarios considered here, the spatial variability in flow resistance among river reaches and floodplains may not be fully captured. These uncertainties may affect flood propagation speed, peak arrival time, and inundation characteristics. In addition, because historical observed discharge, water level, and inundation extent data for comparison are lacking, it is difficult for this study to carry out direct accuracy validation of the simulation results for the Mogangling breach flood scenario. However, many studies have applied IFMS to river flood routing, flash floods, and reservoir breach flood simulation and have compared and tested the results against measured data or post-disaster survey data, all achieving good simulation performance [20,60]. These results provide some reference for the breach flood simulation in this study.

Third, the disaster mitigation benefits of joint operation of the cascade reservoirs are affected by scenario assumptions and actual operating conditions. The upstream inflow-reduction ratio, initial reservoir water levels, and operation rules used in this study correspond to specific engineering and hydrological conditions. The 20% reduction in inflow to the barrier lake by upstream reservoirs represents a reference operation scenario and cannot be directly equated with the regulation capacity attainable under all actual operating conditions. The pre-release scenario for downstream reservoirs assumes that water can be released 24–48 h in advance to create the required storage space. However, actual emergency operation is constrained by the timeliness of monitoring and warning, decision-making and instruction execution times, real-time inflow and forecast errors, discharge facility capacity, allowable drawdown rates, operating conditions of hydraulic and electromechanical equipment, and the safe discharge capacity of downstream channels [61]. These constraints may prevent the pre-release target from being completed within the prescribed time. In addition, the overall storage and regulation performance of the reservoir group depends on coordination among cascade reservoirs [62]. If a key reservoir cannot participate according to the prescribed rules because of equipment failure or operational constraints, the downstream inflow process, peak superposition relationships, and overall disaster mitigation effect may change. The results therefore represent potential mitigation benefits under favorable operating assumptions, and their practical attainability must be evaluated with reference to specific events, real-time operating conditions, and engineering safety constraints.

Fourth, spatial data for hazard-bearing bodies and loss-ratio curves affect estimates of exposure and economic loss. The spatial resolution, reference year, and spatial allocation errors of the population and GDP grids may affect the identification of population and economic activity within inundated areas, particularly where settlements are concentrated in narrow river valleys, and gridded data may not accurately capture spatial differences in these areas [63]. Population and GDP exposure calculated from these data mainly represent the potential scale of affected populations and economic activity and cannot be directly equated with casualties or actual economic losses [64]. For economic losses further estimated using loss-ratio curves, existing curves may not adequately represent the actual vulnerability of hazard-bearing bodies in the Dadu River basin because of differences in building structures, asset types, socioeconomic conditions, and flood characteristics among regions. The reported results are therefore estimates of potential economic loss under the specified scenarios and loss relationships.

Overall, this study primarily conducted scenario simulations based on the reconstruction of a historical event and current engineering conditions, focusing on the potential disaster mitigation effect of breach floods under joint operation of the current cascade reservoirs. Because directly validating data and systematic parameter sensitivity analyses are unavailable, the simulation errors and the relative contributions of different uncertainty factors cannot yet be quantified. Future work should strengthen model calibration and validation by incorporating improved hydrological observations, topographic surveys, modern barrier lake breach cases, and reservoir operation data. Perturbation experiments and uncertainty quantification should also be conducted for key factors such as breach parameters, Manning roughness, and initial reservoir operating conditions. Additional unfavorable scenarios, including insufficient pre-release time, non-participation of key reservoirs, and equipment failure, should be considered to improve the reliability of the study conclusions and their applicability to engineering practice.

5. Conclusions

In this study, the 1786 Mogangling landslide barrier lake in the Dadu River basin was taken as the research object. A numerical model of the barrier lake breach flood was constructed based on IFMS, and a coupled one- and two-dimensional hydrodynamic model was used to reproduce the propagation of the breach flood under natural routing and reservoir impoundment scenarios and to evaluate the disaster mitigation effect under the joint operation of the cascade reservoirs. The main conclusions are as follows:

(1) The total storage capacity of the Mogangling barrier lake is 1.15 billion m^3, and the flood peak discharges of the 300 m and 600 m breach scenarios are 67,100 m^3/s and 128,400 m^3/s, respectively. The breach flood has a high peak and a large volume and is extremely abrupt and destructive; it is a typical above-standard flood that poses a great threat to the flood control safety of the towns along the middle and lower Dadu River and the main Min River.

(2) Under the natural routing scenario without considering reservoir regulation, the breach flood propagates continuously downstream along the Dadu River and finally reaches Yibin, with a propagation distance of about 586.6 km. Under the reservoir impoundment scenario, after successive regulation by the Dagangshan and Longtoushi reservoirs, the flood peak discharge and total flood volume gradually attenuate, and the flood is finally completely retained at the Pubugou reservoir, with a propagation distance of about 140 km. Compared with the natural flood routing scenario, under the joint operation of the cascade reservoirs the flood peak discharges at the cross-sections from Dagangshan to Pubugou are reduced by 30.7–97.9%, and the impact of the breach flood on downstream towns and infrastructure is reduced by 70–89%. This indicates that the joint operation of the cascade reservoirs can significantly reduce the flood peak along the river, greatly reduce the inundation extent and disaster losses, and achieve prominent overall mitigation benefits.

(3) When site conditions permit, excavation of a spillway channel can reduce the storage volume at the onset of breaching and cut the breach flood peak, further reducing the disaster and weakening the disaster-causing capacity of the flood at the source; it is an effective engineering measure in emergency response. When combined with the joint operation of the cascade reservoirs, it can significantly reduce the flood hazard of the downstream area.

Author Contributions: Z.C.: Conceptualization, Methodology, Investigation, Formal analysis, Data curation, Visualization, Writing—original draft, Writing—review and editing. Q.Q.: Investigation, Formal analysis, Writing—original draft, Writing—review and editing. J.F.: Investigation, Formal Analysis, Funding acquisition, Resources, Supervision. J.L. (Jia Li): Conceptualization, Methodology, Supervision, Writing—review and editing. L.D.: Conceptualization, Methodology, Validation, Writing—review and editing. Y.X.: Conceptualization, Methodology, Validation, Writing—review and editing. D.C.: Conceptualization, Funding acquisition, Resources, Supervision, Project administration. J.L. (Jianwei Liu): Conceptualization, Methodology, Supervision, Writing—review and editing. All authors have read and agreed to the published version of the manuscript.

Funding: This research was supported by CHN Energy Investment Group (Grant No. GJNY-DDH-SCZH-2025-001), Yibin Science and Technology Program (Grant No. 26JBGSFZLX0002) and Sichuan Provincial Water and Drought Disaster Prevention Capacity Enhancement Project (Grant No. N5100012023000037).

Data Availability Statement: The land use data, population and GDP grid data were obtained from the Resource and Environment Data Cloud Platform (https://www.resdc.cn/) (accessed on 10 March 2026). The building data were obtained from the National Tibetan Plateau Data Center (https://data.tpdc.ac.cn) (accessed on 14 March 2026).

Acknowledgments: The authors acknowledge the Sichuan Provincial Water Resources Department for providing data support.

Conflicts of Interest: Authors Zaini Chen, Jia Li, and Liudan Ding were employed by the company China Energy Dadu River Hydropower Development Co., Ltd. Author Jing Fu was employed by the company Engineering Design & Research Institute of Sichuan University Co., Ltd. The authors declare that this study received funding from CHN Energy Investment Group (Grant No. GJNY-DDH-SCZH-2025-001). The funder was not involved in the study design, collection, analysis, interpretation of data, the writing of this article, or the decision to submit it for publication. The remaining authors declare that the research was conducted in the absence of any commercial or financial relationships that could be construed as a potential conflict of interest.

References

1. Zhong, Q.; Chen, X.; Mei, S.; Shan, Y.; Du, Z. A state of the art review on the failure risk and process of the landslide-induced dammed lake. *Adv. Water Sci* **2022**, *33*, 659–670. (In Chinese) https://doi.org/10.14042/j.cnki.32.1309.2022.04.013
2. Fan, X.; Dufresne, A.; Siva Subramanian, S.; Strom, A.; Hermanns, R.; Tacconi Stefanelli, C.; Hewitt, K.; Yunus, A.P.; Dunning, S.; Capra, L.; et al. The Formation and Impact of Landslide Dams—State of the Art. *Earth Sci. Rev.* **2020**, *203*, 103116. https://doi.org/10.1016/j.earscirev.2020.103116.
3. Zhong, Q.; Wang, L.; Chen, S.; Chen, Z.; Shan, Y.; Zhang, Q.; Ren, Q.; Mei, S.; Jiang, J.; Hu, L.; et al. Breaches of Embankment and Landslide Dams—State of the Art Review. *Earth Sci. Rev.* **2021**, *216*, 103597. https://doi.org/10.1016/j.earscirev.2021.103597.
4. Li, J.; Cao, Z.; Cui, Y.; Fan, X.; Yang, W.; Huang, W.; Borthwick, A. Hydro-Sediment-Morphodynamic Processes of the Baige Landslide-Induced Barrier Lake, Jinsha River, China. *J. Hydrol.* **2021**, *596*, 126134. https://doi.org/10.1016/j.jhydrol.2021.126134.
5. Liu, W.; Carling, P.A.; Hu, K.; Wang, H.; Zhou, Z.; Zhou, L.; Liu, D.; Lai, Z.; Zhang, X. Outburst Floods in China: A Review. *Earth Sci. Rev.* **2019**, *197*, 102895. https://doi.org/10.1016/j.earscirev.2019.102895.
6. Zhang, Y.; Zhu, L.; Yang, W.; Luo, H.; Jiang, L.; He, D.; Liu, J. High resolution rapid climate change records of lacustrine deposits of Diexi Basin in the eastern margin of Qingha-i Tibet Plateau, 40-30ka BP. *Earth Sci. Front.* **2009**, *16*, 91–98. (In Chinese)
7. Zhang, Y.; Li, H.; Li, J. Impact of the 30–40 ka B.P. Warm-humid Climate in Tibet on the Geo-environment of the Deep-incised River Valleys in West Sichuan. *Acta Geosci. Sin.* **2016**, *37*, 481–492. (In Chinese)
8. Chen, J.; Dai, F.; Lv, T.; Cui, Z. Holocene Landslide-Dammed Lake Deposits in the Upper Jinsha River, SE Tibetan Plateau and Their Ages. *Quat. Int.* **2013**, *298*, 107–113. https://doi.org/10.1016/j.quaint.2012.09.018.
9. Chen, J.; Cui, Z. Discovery of Outburst Deposits Induced by the Xuelongnang Paleolandslide-Dammed Lake in the Upper Jinsha River,China and Its Environmental and Hazard Significance. *Acta Sedimentol. Sin.* **2015**, *33*, 275–284. (In Chinese) https://doi.org/10.14027/j.cnki.cjxb.2015.02.007
10. Dai, F.C.; Lee, C.F.; Deng, J.H.; Tham, L.G. The 1786 Earthquake-Triggered Landslide Dam and Subsequent Dam-Break Flood on the Dadu River, Southwestern China. *Geomorphology* **2005**, *65*, 205–221. https://doi.org/10.1016/j.geomorph.2004.08.011.
11. Cui, S.; Wu, H.; Pei, X.; Yang, Q.; Huang, R.; Guo, B. Characterizing the Spatial Distribution, Frequency, Geomorphological and Geological Controls on Landslides Triggered by the 1933 Mw 7.3 Diexi Earthquake, Sichuan, China. *Geomorphology* **2022**, *403*, 108177. https://doi.org/10.1016/j.geomorph.2022.108177.
12. Cui, P.; Zhu, Y.; Han, Y.; Chen, X.; Zhuang, J. The 12 May Wenchuan Earthquake-Induced Landslide Lakes: Distribution and Preliminary Risk Evaluation. *Landslides* **2009**, *6*, 209–223. https://doi.org/10.1007/s10346-009-0160-9.
13. Cui, P.; Dang, C.; Zhuang, J.; You, Y.; Chen, X.; Scott, K.M. Landslide-Dammed Lake at Tangjiashan, Sichuan Province, China (Triggered by the Wenchuan Earthquake, May 12, 2008): Risk Assessment, Mitigation Strategy, and Lessons Learned. *Environ. Earth Sci.* **2012**, *65*, 1055–1065. https://doi.org/10.1007/s12665-010-0749-2.
14. Liu, D.; Cui, Y.; Wang, H.; Jin, W.; Wu, C.; Bazai, N.A.; Zhang, G.; Carling, P.A.; Chen, H. Assessment of Local Outburst Flood Risk from Successive Landslides: Case Study of Baige Landslide-Dammed Lake, Upper Jinsha River, Eastern Tibet. *J. Hydrol.* **2021**, *599*, 126294. https://doi.org/10.1016/j.jhydrol.2021.126294.
15. Zhong, Q.; Chen, S.; Shan, Y. Prediction of the Overtopping-Induced Breach Process of the Landslide Dam. *Eng. Geol.* **2020**, *274*, 105709. https://doi.org/10.1016/j.enggeo.2020.105709.
16. Zhong, H.; Zhang, B.; Ma, T.; Qi, X.; Wang, X.; Shang, H.; Qu, S.; Fang, W. Flood Scenario Simulation, Based on the Hydrological and Hydrodynamic Model in the Puyang River Catchment. *Water* **2022**, *14*, 3873. https://doi.org/10.3390/w14233873.

17. Nguyen, H.D.; Dang, D.K.; Nguyen, N.Y.; Pham Van, C.; Van Nguyen, T.T.; Nguyen, Q.-H.; Nguyen, X.L.; Pham, L.T.; Pham, V.T.; Bui, Q.-T. Integration of Machine Learning and Hydrodynamic Modeling to Solve the Extrapolation Problem in Flood Depth Estimation. *J. Water Clim. Change* **2024**, *15*, 284–304. https://doi.org/10.2166/wcc.2023.573.
18. Namara, W.G.; Damisse, T.A.; Tufa, F.G. Application of HEC-RAS and HEC-GeoRAS Model for Flood Inundation Mapping, the Case of Awash Bello Flood Plain, Upper Awash River Basin, Oromiya Regional State, Ethiopia. *Model. Earth Syst. Environ.* **2022**, *8*, 1449–1460. https://doi.org/10.1007/s40808-021-01166-9.
19. Annis, S.; Badas, M.G.; Mascaro, G. Increasing the Fidelity of Hyperlocal Simulations of Urban Pluvial Flooding through Street Flooding Observations. *Adv. Water Resour.* **2026**, *209*, 105223. https://doi.org/10.1016/j.advwatres.2026.105223.
20. Qin, Q.; Cao, D.; Liu, J.; Wang, T.; Xu, W.; Lv, J. Runoff Simulation and Flood Risk Assessment of Heavy Rainfall-Flood Events in the Juhe River Basin, Beijing. *Environ. Earth Sci.* **2026**, *85*, 378. https://doi.org/10.1007/s12665-026-13120-y.
21. Chen, C.; Zhang, L.; Xiao, T.; He, J. Barrier Lake Bursting and Flood Routing in the Yarlung Tsangpo Grand Canyon in October 2018. *J. Hydrol.* **2020**, *583*, 124603. https://doi.org/10.1016/j.jhydrol.2020.124603.
22. Mei, S.; Chen, S.; Zhong, Q.; Shan, Y. Detailed Numerical Modeling for Breach Hydrograph and Morphology Evolution during Landslide Dam Breaching. *Landslides* **2022**, *19*, 2925–2949. https://doi.org/10.1007/s10346-022-01952-1.
23. Zhang, J.; Yang, X.; Fan, G.; Li, H.; Zhou, J. Physical and Numerical Modeling of a Landslide Dam Breach and Flood Routing Process. *J. Hydrol.* **2024**, *628*, 130552. https://doi.org/10.1016/j.jhydrol.2023.130552.
24. Ma, J.; Xu, C.; Chen, J. Dam-Breach Process Simulation and Risk Assessment of Outburst Flood Induced by the Tangjiashan Landslide-Dammed Lake. *J. Hydrol. Reg. Stud.* **2025**, *57*, 102164. https://doi.org/10.1016/j.ejrh.2024.102164.
25. Chenyu, F.; Ke, L.; Wang, J.; Best, J.; Zhang, Y.; Sheng, Y.; Liu, K.; Chen, T.; Zeng, F.; Zhan, P.; et al. Exacerbating Dam-Induced Fragmentation in China's River Systems. *Commun. Earth Environ.* **2025**, *6*, 428. https://doi.org/10.1038/s43247-025-02416-9.
26. Chen, G.; Zhao, X.; Zhou, Y.; Guo, S.; Xu, C.-Y.; Chang, F.-J. Emergency Disposal Solution for Control of a Giant Landslide and Dammed Lake in Yangtze River, China. *Water* **2019**, *11*, 1939. https://doi.org/10.3390/w11091939.
27. Gan, B.-R.; Yang, X.-G.; Liao, H.-M.; Zhou, J.-W. Flood Routing Process and High Dam Interception of Natural Discharge from the 2018 Baige Landslide-Dammed Lake. *Water* **2020**, *12*, 605. https://doi.org/10.3390/w12020605.
28. Zhang, Q.; Chen, Z.; Li, Y.; Yu, S.; Wang, L.; Zhou, X.; Wu, S. Quantitative Assessment on Landslide Dam Risks and Mitigation: An in-Depth Study on the Baige Lake Breach. *Environ. Earth Sci.* **2023**, *82*, 96. https://doi.org/10.1007/s12665-023-10778-6.
29. Wang, B.; Yang, S.; Chen, C. Landslide Dam Breaching and Outburst Floods: A Numerical Model and Its Application. *J. Hydrol.* **2022**, *609*, 127733. https://doi.org/10.1016/j.jhydrol.2022.127733.
30. Liu, P.; Zhang, Z.; Tang, L.; Cao, Y. Impacts of Basin-Wide Reservoir Operations on Future Yangtze River Flood and Flow Regimes under Bias-Corrected CMIP6 Projections. *J. Hydrol. Reg. Stud.* **2026**, *65*, 103446. https://doi.org/10.1016/j.ejrh.2026.103446.
31. Yang, N.; Zhang, T.; Li, J.; Feng, P. Improved Comprehensive Flood Risk Index Method and Multi-Scenario Flood Simulation for Downstream Area of the Reservoir. *Water Resour. Manag.* **2026**, *40*, 48. https://doi.org/10.1007/s11269-025-04370-9.
32. Zhao, X.; Liu, C.; Wang, W.; Gu, B.; Yang, K.; Zhang, M.; Ma, J. Dam break flood simulation of sheyuegou reservoir and reasons for the dam break. *China Rural Water Hydrop.* 2022, 171–177. (In Chinese)
33. Zhao, B.; Wang, Y.; Wu, J.; Su, L.; Liu, J.; Jin, G. The Mogangling Giant Landslide Triggered by the 1786 Moxi M 7.75 Earthquake, China. *Nat. Hazard.* **2021**, *106*, 459–485. https://doi.org/10.1007/s11069-020-04471-1.
34. Xue, R.; Zhang, X.; Cai, Y.; Wang, M.; Deng, Q.; Zhang, H.; Kawaike, K. Numerical Simulation of Landslide Dam Overtopping Failure Considering Headward Erosion. *J. Hydrol.* **2021**, *601*, 126608. https://doi.org/10.1016/j.jhydrol.2021.126608.
35. Huang, Q.; Duanmu, X.; Shang, H.; Xu, A.; Zhong, H. Flood Risk Assessment Using Coupled 1D–2D Hydrodynamic Models: A Case Study of the Qujiang River Basin. *Water* **2026**, *18*, 1198. https://doi.org/10.3390/w18101198.
36. Zhang, B.; Qin, J.; Wang, Z.; Zhao, L.; Wang, L.; Ma, W. Coupling Delphi-Driven Expert Elicitation with Bayesian Networks in GIS: An Advanced Approach to Quantifying and Mapping River Flood Risk. *Water* **2026**, *18*, 2072. https://doi.org/10.3390/w18172072.
37. Shen, H.; Cao, D.; Wan, H.; Liu, S.; Yang, Y.; Zheng, L.; Hou, Y.; Zhao, C.; Cheng, D. 1-D and 2-D coupling model and reservoir regulation-based analysis on flood encounter and inundation of Yibin Reach of Yangtze River. *Water Resour. Hydropower Eng.* **2023**, *54*, 1–21. (In Chinese) https://doi.org/10.13928/j.cnki.wrahe.2023.04.001
38. Beden, N.; Orhan, O.; Peker, İ.B.; Gülbaz, S.; Demir, V. Impact on the Spatial Interpretation of Flood Hazard: Evaluating Depth and Depth–Velocity Classification Logics. In *Flood Risk—Assessment, Management Strategies, and Emerging Technologies*; Demir, V., Beden, N., Orhan, O., Eds.; IntechOpen: London, UK, 2026; Volume 16.

39. Peker, İ.B.; Gülbaz, S.; Demir, V.; Orhan, O.; Beden, N. Integration of HEC-RAS and HEC-HMS with GIS in Flood Modeling and Flood Hazard Mapping. *Sustainability* **2024**, *16*, 1226. https://doi.org/10.3390/su16031226.
40. Wing, O.E.J.; Pinter, N.; Bates, P.D.; Kousky, C. New Insights into US Flood Vulnerability Revealed from Flood Insurance Big Data. *Nat. Commun.* **2020**, *11*, 1444. https://doi.org/10.1038/s41467-020-15264-2.
41. Merz, B.; Kreibich, H.; Schwarze, R.; Thieken, A. Assessment of Economic Flood Damage. *Nat. Hazards Earth Syst. Sci.* **2010**, *10*, 1697–1724. https://doi.org/10.5194/nhess-10-1697-2010.
42. Jongman, B.; Kreibich, H.; Apel, H.; Barredo, J.I.; Bates, P.D.; Feyen, L.; Gericke, A.; Neal, J.; Aerts, J.C.J.H.; Ward, P.J. Comparative Flood Damage Model Assessment: Towards a European Approach. *Nat. Hazards Earth Syst. Sci.* **2012**, *12*, 3733–3752. https://doi.org/10.5194/nhess-12-3733-2012.
43. Junfeng, W.; Yunsheng, W.; Simeng, D.; Yun, C.; Lei, W. Genetic Mechanism and Failure Process of the Mogangling Seismic Landslide. *J. Geol. Soc. India* **2013**, *82*, 277–282. https://doi.org/10.1007/s12594-013-0150-3.
44. Thackeray, C.W.; Hall, A.; Norris, J.; Chen, D. Constraining the Increased Frequency of Global Precipitation Extremes under Warming. *Nat. Clim. Change* **2022**, *12*, 441–448. https://doi.org/10.1038/s41558-022-01329-1.
45. Fischer, E.M. Increasing Probability of Record-Shattering Climate Extremes. *Nat. Clim. Change* **2021**, *11*, 689–695. https://doi.org/10.1038/s41558-021-01092-9.
46. Shazil, M.S.; Bogaard, T.; Greco, R. Hydrological Perspective of Landslide Dams: A Review. *Nat. Hazard.* **2026**, *122*, 620. https://doi.org/10.1007/s11069-026-08393-2.
47. Liu, Z.; Chen, Q.; Wang, C.; Zhou, C.; Li, X.; Chen, C. Experimental Investigation on Failure Processes and Characteristics of Landslide Dams with Different Inflow Conditions. *Sci. Rep.* **2025**, *15*, 7546. https://doi.org/10.1038/s41598-025-89464-5.
48. Zhu, L.; Li, S.; Dong, B.; Xu, Q.; Yuan, J. Effect of Baige landslide-dammed lake on runoff and sediment of the Jinsha River and operation of cascade reservoirs. *J. Lake Sci.* **2020**, *32*, 1165–1176. (In Chinese)
49. Chou, F.N.-F.; Wu, C.-W. Expected Shortage Based Pre-Release Strategy for Reservoir Flood Control. *J. Hydrol.* **2013**, *497*, 1–14. https://doi.org/10.1016/j.jhydrol.2013.05.039.
50. Zhang, H.; Dou, Y.; Ye, L.; Zhang, C.; Yao, H.; Bao, Z.; Tang, Z.; Wang, Y.; Huang, Y.; Zhu, S.; et al. Realizing the Full Reservoir Operation Potential during the 2020 Yangtze River Floods. *Sci. Rep.* **2022**, *12*, 2822. https://doi.org/10.1038/s41598-022-06801-8.
51. Loc, H.H.; Emadzadeh, A.; Park, E.; Nontikansak, P.; Deo, R.C. The Great 2011 Thailand Flood Disaster Revisited: Could It Have Been Mitigated by Different Dam Operations Based on Better Weather Forecasts? *Environ. Res.* **2023**, *216*, 114493. https://doi.org/10.1016/j.envres.2022.114493.
52. Liu, N.; Chen, Z.; Zhang, J.; Lin, W.; Chen, W.; Xu, W. Draining the Tangjiashan Barrier Lake. *J. Hydraul. Eng.* **2010**, *136*, 914–923. https://doi.org/10.1061/(ASCE)HY.1943-7900.0000241.
53. Zhou, X.; Du, X.; Zhou, J.; Yang, Z.; Jiang, T.; Chen, W. Draining the Successive Baige Barrier Lakes, China: Insight into the Emergency Response. *Nat. Hazard. Rev.* **2024**, *25*, 05024006. https://doi.org/10.1061/NHREFO.NHENG-2052.
54. Baker, V.R. Paleoflood Hydrology: Origin, Progress, Prospects. *Geomorphology* **2008**, *101*, 1–13. https://doi.org/10.1016/j.geomorph.2008.05.016.
55. Wahl, T.L. Uncertainty of Predictions of Embankment Dam Breach Parameters. *J. Hydraul. Eng.* **2004**, *130*, 389–397. https://doi.org/10.1061/(ASCE)0733-9429(2004)130:5(389).
56. Froehlich, D.C. Embankment Dam Breach Parameters and Their Uncertainties. *J. Hydraul. Eng.* **2008**, *134*, 1708–1721. https://doi.org/10.1061/(ASCE)0733-9429(2008)134:12(1708).
57. Gilvear, D.J.; Winterbottom, S.J. Channel Change and Flood Events since 1783 on the Regulated River Tay, Scotland: Implications for Flood Hazard Management. *Regul. RiversRes. Manag.* **1992**, *7*, 247–260. https://doi.org/10.1002/rrr.3450070304.
58. Liu, J.; You, Y.; Zhang, Q.; Gu, X. Attribution of Streamflow Changes across the Globe Based on the Budyko Framework. *Sci. Total Environ.* **2021**, *794*, 148662. https://doi.org/10.1016/j.scitotenv.2021.148662.
59. Wang, H.; Liu, Z.; Feng, J.; Zhang, P.; Liu, R.; Wang, S. Hydrodynamic Effects of Flash Floods Considering the Bridges and Their Blockage in South China. *J. Flood Risk Manag.* **2025**, *18*, e70086. https://doi.org/10.1111/jfr3.70086.
60. Yang, N.; Zhang, T.; Li, J.; Feng, P.; Zhu, C. Spatial Heterogeneity and Multivariate Drivers of Flood Hazard in Data-Scarce Small Watersheds. *J. Hydrol. Reg. Stud.* **2026**, *65*, 103479. https://doi.org/10.1016/j.ejrh.2026.103479.
61. Wei, G.; Liang, G.; Ding, W.; He, B.; Wu, J.; Ren, M.; Zhou, H. Deriving Optimal Operating Rules for Flood Control Considering Pre-Release Based on Forecast Information. *J. Hydrol.* **2022**, *615*, 128665. https://doi.org/10.1016/j.jhydrol.2022.128665.
62. Chen, J.; Zhong, P.; Wang, M.; Zhu, F.; Wan, X.; Zhang, Y. A Risk-Based Model for Real-Time Flood Control Operation of a Cascade Reservoir System under Emergency Conditions. *Water* **2018**, *10*, 167. https://doi.org/10.3390/w10020167.

63. Leyk, S.; Gaughan, A.E.; Adamo, S.B.; De Sherbinin, A.; Balk, D.; Freire, S.; Rose, A.; Stevens, F.R.; Blankespoor, B.; Frye, C.; et al. The Spatial Allocation of Population: A Review of Large-Scale Gridded Population Data Products and Their Fitness for Use. *Earth Syst. Sci. Data* **2019**, *11*, 1385–1409. https://doi.org/10.5194/essd-11-1385-2019.
64. Fox, S.; Agyemang, F.; Hawker, L.; Neal, J. Integrating Social Vulnerability into High-Resolution Global Flood Risk Mapping. *Nat. Commun.* **2024**, *15*, 3155. https://doi.org/10.1038/s41467-024-47394-2.

Disclaimer/Publisher's Note: The statements, opinions and data contained in all publications are solely those of the individual author(s) and contributor(s) and not of MDPI and/or the editor(s). MDPI and/or the editor(s) disclaim responsibility for any injury to people or property resulting from any ideas, methods, instructions or products referred to in the content.